

# 000 001 002 003 004 005 REVISITING GLOBAL TEXT CONDITIONING IN 006 DIFFUSION TRANSFORMERS 007 008 009

010 **Anonymous authors**  
011 Paper under double-blind review  
012  
013  
014  
015  
016  
017  
018  
019  
020  
021  
022  
023

## ABSTRACT

024 Diffusion transformers typically incorporate textual information via (i) attention  
025 layers and (ii) a modulation mechanism using a pooled text embedding. Never-  
026 theless, recent approaches discard modulation-based text conditioning and rely  
027 exclusively on attention. In this paper, we address **whether modulation-based**  
028 **text conditioning is necessary and whether it can provide any performance ad-**  
029 **vantage**. Our analysis shows that, in its conventional usage, the pooled embedding  
030 contributes little to overall performance, suggesting that attention alone is generally  
031 sufficient for faithfully propagating prompt information. However, we reveal that  
032 the pooled embedding can provide significant gains when used from a different  
033 perspective—serving as guidance and enabling controllable shifts toward more  
034 desirable properties. This approach is training-free, simple to implement, incurs  
035 negligible runtime overhead, and can be applied to various diffusion models, bring-  
036 ing improvements across diverse tasks, including text-to-image/video generation  
037 and image editing.  
038

## 1 INTRODUCTION

039 Since the pioneering works on diffusion models (DMs) (Ho et al., 2020; Song et al., 2020), the  
040 UNet architecture (Ronneberger et al., 2015) has served as the dominant backbone for diffusion-  
041 based image generation. This trend extended to text-to-image models (Saharia et al., 2022; Nichol  
042 et al., 2021), which employ UNet-based architectures (Rombach et al., 2022) and incorporate the  
043 CLIP text encoder (Radford et al., 2021) to condition the model on text sequences through the  
044 attention mechanism (Vaswani et al., 2017). Later, models such as Podell et al. (2023) began to  
045 incorporate the pooled CLIP embedding via modulation mechanisms (Karras et al., 2017; 2019),  
046 in addition to the token-wise text embeddings. More recently, works including Labs et al. (2025);  
047 Labs (2024); Esser et al. (2024); Kong et al. (2024); Cai et al. (2025) have adopted transformer-based  
048 architectures (Peebles & Xie, 2023) while retaining modulation-based text conditioning. Recent  
049 models (Wan et al., 2025; Wu et al., 2025; Agarwal et al., 2025; Xie et al., 2024) discard global text  
050 conditioning, achieving comparable text alignment by relying solely on attention. This transition  
051 raises questions about the role and necessity of global text conditioning, which we aim to explore.  
052

053 We observe that, at first glance, modulation-based text conditioning appears non-contributory, and  
054 attention alone is sufficient to capture textual information. However, we argue that it is premature to  
055 discard global text conditioning and that it should instead be leveraged from a different perspective.  
056 Specifically, we draw inspiration from the interpretability of the modulation mechanism (Karras et al.,  
057 2019) and the ability of CLIP to control it (Garibi et al., 2025). We suggest that the pooled text  
058 embedding can act as a corrector, adjusting the diffusion trajectory toward better modes.

059 In summary, our contributions are as follows: **(1)** We conduct an in-depth analysis of global text  
060 conditioning in contemporary DMs and find that it plays only a minor role relative to attention-based  
061 text conditioning. **(2)** We show that global text conditioning can yield significant improvements when  
062 viewed from the perspective of *modulation guidance*. Furthermore, we enhance its effectiveness by  
063 proposing dynamic strategies. **(3)** We introduce techniques for integrating the pooled embedding  
064 into fully attention-based models, thereby improving their performance via modulation guidance. **(4)**  
065 From a practical standpoint, our approach is simple to implement, incurs negligible overhead, and  
066 delivers performance gains on state-of-the-art multi- and few-step DMs across text-to-image/video  
067 and image-editing tasks.

054 **2 RELATED WORK**

055

056 Several post-training approaches have been proposed to improve DM quality. The first group centers  
 057 on *classifier-free guidance (CFG) modifications* (Ho & Salimans, 2022). Specifically, prior works im-  
 058 prove CFG by optimizing scale factors (Fan et al., 2025), addressing off-manifold challenges (Chung  
 059 et al., 2024), modifying the unconditional branch (Karras et al., 2024), mitigating oversaturation at  
 060 high CFG scales (Sadat et al., 2024; 2025; Lin et al., 2024), and introducing dynamic CFG strate-  
 061 gies (Kynkänniemi et al., 2024; Sadat et al., 2023; Wang et al., 2024; Yehezkel et al., 2025). In  
 062 contrast, our method complements CFG and, importantly, can also be applied to few-step DMs (Song  
 063 et al., 2023; Sauer et al., 2024b; Yin et al., 2024a; Starodubcev et al., 2025) that do not use CFG.

064 The second group focuses on *test-time optimization*. A dominant line of work (Chefer et al., 2023; Seo  
 065 et al., 2025; Yiflach et al., 2025; Li et al., 2023; Rassin et al., 2023; Agarwal et al., 2023; Dahary et al.,  
 066 2024; Marioriyad et al., 2025; Binyamin et al., 2025; Phung et al., 2024; Chen et al., 2024; Kwon  
 067 et al., 2022) relies on handcrafted loss functions, typically guided by heuristics about how attention  
 068 maps should behave, and optimizes these maps accordingly. Other methods focus on optimizing only  
 069 the initial noise rather than the full denoising trajectory (Eyring et al., 2025; Ma et al., 2025a; Eyring  
 070 et al., 2024; Guo et al., 2024), or on fine-tuning LoRAs to extract different concepts (Gandikota et al.,  
 071 2024). In contrast, our approach avoids complex loss design and intensive model tuning while still  
 072 improving performance.

073 Finally, works most closely related to ours are *attention guidance methods*. These methods (Chen  
 074 et al., 2025; Hong et al., 2023; Ahn et al., 2025; Nguyen et al., 2024) leverage positive and negative  
 075 prompts, compute attention outputs for both, and perform controlled extrapolation in the attention  
 076 space—pushing the model toward positive prompts and away from negative ones. Our approach also  
 077 relies on guidance in feature space but applies it through a small MLP rather than through attention.

078 **3 MODULATION LAYERS**

079

080 In this section, we briefly recap the key components of modulation layers used in transformer DMs.

081 State-of-the-art text-to-image DMs (Labs, 2024; Cai et al., 2025) typically represent images as  
 082 sequences of continuous tokens, aligning them with text tokens in a unified representation. This  
 083 combined sequence is processed through a series of transformer blocks (Peebles & Xie, 2023),  
 084 which primarily consist of MLPs, normalization, and attention layers. To condition the model on  
 085 a text prompt, two types of encoders are usually used: a T5 (Raffel et al., 2020) and a CLIP text  
 086 encoder (Radford et al., 2021), which operate as follows:

$$y(\mathbf{p}, t) = \text{MLP}(t, \text{CLIP}(\mathbf{p})), \quad \mathbf{s} = [\text{T5}(\mathbf{p}), \mathbf{x}], \quad (1)$$

087 Here,  $y$  denotes a global conditioning vector derived from the time step  $t$  and the pooled embedding  
 088 of the prompt  $\mathbf{p}$ , whereas  $\mathbf{s}$  denotes the concatenated sequence of image tokens  $\mathbf{x}$  and text tokens  
 089  $\text{T5}(\mathbf{p})$ . The sequence  $\mathbf{s}$  is then processed via cross-attention to incorporate text information, while  
 090 the global conditioning vector  $y$  is shared across the entire model and constructs a modulation space  
 091 that influences the modulation layers.

$$\text{Mod}(\mathbf{s}, y) = \alpha_s(y) \cdot \mathbf{s} + \beta_s(y), \quad (2)$$

092 Here,  $\alpha_s$  and  $\beta_s$  are the coefficients of the modulation layer, representing scaling and shifting  
 093 operations, respectively. Notably, modulation layers have proved effective in enabling semantic  
 094 control and transformation in GANs (Karras et al., 2019; 2020; 2021). In DMs, they have been  
 095 used to address image editing problems (Garibi et al., 2025; Dalva et al., 2024). While these layers  
 096 have shown effectiveness in semantic control tasks, their role in improving image generation quality  
 097 remains unexplored.

103 **4 ANALYSIS OF THE POOLED TEXT EMBEDDING ROLE**

104

105 In recent DMs, there is a trend to discard the pooled text embedding and rely solely on the timestep  
 106  $t$  to produce  $y$ , i.e.,  $\text{MLP}(t, \text{CLIP}(\mathbf{p})) \rightarrow \text{MLP}(t)$ . In this setup, the text is incorporated only  
 107 through the text encoder T5. However, no strict justification for this design choice has been provided.

Configuration		CLIP Score $\uparrow$	PickScore $\uparrow$	ImageReward $\uparrow$
<b>FLUX schnell</b>				
Initial,	short	30.1	21.6	6.2
w/o CLIP,	short	29.0 <b>(-1.1)</b>	21.3 <b>(-0.3)</b>	4.5 <b>(-1.7)</b>
w/o T5,	short	28.9 <b>(-1.2)</b>	21.0 <b>(-0.6)</b>	1.5 <b>(-4.7)</b>
Initial,	long	33.1	21.0	10.3
w/o CLIP,	long	32.8 <b>(-0.3)</b>	21.0 <b>(-0.0)</b>	10.4 <b>(+0.1)</b>
w/o T5,	long	30.7 <b>(-2.4)</b>	19.9 <b>(-1.1)</b>	2.4 <b>(-7.9)</b>
<b>HiDream-Fast</b>				
Initial,	short	30.3	21.8	7.9
w/o CLIP,	short	30.3 <b>(-0.0)</b>	21.8 <b>(-0.0)</b>	8.1 <b>(+0.1)</b>
w/o Llama,	short	20.2 <b>(-10.1)</b>	18.2 <b>(-3.6)</b>	-21.5 <b>(-29.4)</b>
Initial,	long	32.9	21.5	12.8
w/o CLIP,	long	32.9 <b>(-0.0)</b>	21.5 <b>(-0.0)</b>	13.0 <b>(+0.2)</b>
w/o Llama,	long	16.8 <b>(-16.1)</b>	16.0 <b>(-4.5)</b>	-20.8 <b>(-33.6)</b>

Table 1: Image quality results for short and long prompts. The CLIP embedding does not affect output quality on long prompts for **FLUX schnell** and has no effect for **HiDream-Fast**.

Therefore, in this section, we investigate the impact of the pooled embedding on the generative performance of DMs.

**Influence of the CLIP pooled embedding.** First, we analyze the influence of CLIP on text-to-image generation performance. To this end, we examine two contemporary models: FLUX schnell and HiDream-Fast. Specifically, we analyze the impact of CLIP by removing the pooled embedding, setting  $\text{CLIP}(p) \rightarrow 0$ , and comparing it to the standard case with CLIP enabled. Our key observation is that **the pooled CLIP embedding is partially inactive in FLUX schnell and fully inactive in HiDream-Fast**.

Specifically, we find that the influence of CLIP in **FLUX schnell** is inconsistent: it is negligible for long prompts but can be impactful for short ones. To confirm this, we construct two subsets of prompts (1K each) from the MJHQ dataset (Li et al., 2024): short (10 tokens) and long (77 tokens). We then evaluate the DM’s performance on each subset. In Table 1 (top), we report image quality metrics (CLIP Score, PickScore, and ImageReward) for each subset. We observe that for long prompts, CLIP has little effect, with only a minimal impact on quality. In contrast, for short prompts, its influence is more pronounced.

Moreover, in Figure 1, we analyze the difference between images generated with and without CLIP as a function of prompt length (measured by the number of tokens). We find that for longer prompts, the deviation from the initial generation becomes negligible, and the images fully resemble the initial ones, as visually confirmed in Figure 1 (bottom).

For **HiDream-Fast**, we observe slightly different behavior: the CLIP pooled embedding exhibits no effect for either short or long prompts, as numerically confirmed in Table 1 (bottom).

**Influence of the pooled embedding on other models.** Additionally, we explore the reintegration of CLIP into a DM from which it was originally absent. To this end, we consider the COSMOS model (Agarwal et al., 2025) and incorporate the CLIP pooled embedding into it as described in Section 5. In this case, we observe the same behavior as with the HiDream-Fast model: CLIP has no influence. This result is numerically confirmed in Section 6. Finally, in Appendix A, we observe the same effect in the instruction-guided image editing task performed with the FLUX Kontext model. In Section 6, we show that this limitation can result in insufficient editing strength for complex cases.

## 5 MODULATION GUIDANCE

Our observations raise questions about the necessity of using the pooled embedding in generative tasks. **However, although the pooled text embedding may seem uninformative in some cases, we propose reconsidering its role from a different perspective—one that can lead to improved generative performance in DMs.**

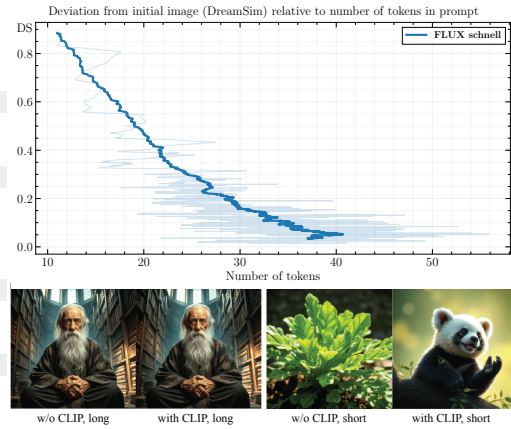


Figure 1: (top) Difference between images (DreamSim) with and without CLIP as a function of prompt length. (bot) For long prompts, images without CLIP generally do not differ from the initial ones.

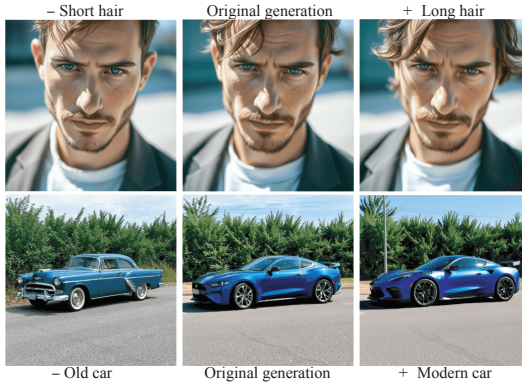
162 **Guidance in modulation space.** We draw inspiration from the understanding that modulation layers  
 163 can drive semantic changes in generated images (Karras et al., 2019). Moreover, the CLIP encoder  
 164 is trained to construct a shared space between images and text, resulting in interpretable geometry.  
 165 Thus, we suggest that CLIP enables interpretable modifications of the modulation space using natural  
 166 language and guides the model toward modes with more desirable properties.

167 We propose a training-free, plug-and-play technique to reactivate CLIP and strengthen its influence  
 168 during generation, drawing inspiration from Garibi et al. (2025). Specifically, we amplify its effect  
 169 by introducing guidance in the modulation space.

$$171 \mathbf{y}(\mathbf{p}, t) \rightarrow \hat{\mathbf{y}}(\mathbf{p}, \mathbf{p}_+, \mathbf{p}_-, t) = \mathbf{y}(\mathbf{p}, t) + w \cdot (\mathbf{y}(\mathbf{p}_+, t) - \mathbf{y}(\mathbf{p}_-, t)). \quad (3)$$

173 We note that  $\hat{\mathbf{y}}$  affects only the modulation coefficients and is shared across all DM blocks, thereby  
 174 incurring negligible computational overhead compared to basic generation. Moreover, this technique  
 175 can be applied on top of CFG guidance or with distilled DMs that do not rely on CFG.

176 To provide intuition behind the guidance, we  
 177 first analyze it from the perspective of se-  
 178 mantic changes. Prior work has focused on  
 179 identifying interpretable directions in DMs,  
 180 either through supervised (Gandikota et al.,  
 181 2024) or unsupervised approaches (Gandikota  
 182 et al., 2025). In contrast, we demonstrate that  
 183 such interpretable directions are already em-  
 184 bedded within the model and can be accessed  
 185 by shifting in the modulation space. Speci-  
 186 cally, in Figure 2, we consider two exam-  
 187 ples:  $\mathbf{p}_+ = \text{Long hair}$ ; Modern car  
 188 and  $\mathbf{p}_- = \text{Short hair}$ ; Old car. We ob-  
 189 serve that the pooled embedding can substan-  
 190 tially influence the generated image, leading to  
 191 both local (hair length) and global (car style)  
 192 changes.



193 Figure 2: The modulation guidance enables local (top)  
 194 and global (bottom) changes and encourages its use to  
 195 shift a DM toward modes with better properties.

196 Our observations suggest that modulation guidance provides an additional degree of freedom in  
 197 generation, beyond what CFG offers. Building on this, we propose using it to enhance generation  
 198 quality across multiple dimensions. Specifically, we consider **general changes: aesthetics,**  
 199 **complexity,** and **specific changes: hands correction, object counting, color,**  
 200 **position.** For the latter, we focus on common criteria typically measured in T2I benchmarks  
 201 (Ghosh et al., 2023). Notably, our technique requires only the selection of a suitable prompt  
 202 for each category—no additional training or fine-tuning is necessary. In Appendix D, we present the  
 203 prompts used for each targeted aspect.

204 **Dynamic modulation guidance.** We find that a constant guidance scale  $w$  is generally effective,  
 205 but excessively high values can overweight the prompt and cause the model to neglect textual  
 206 information (Appendix C). To address this, we draw inspiration from dynamic CFG (Sadat et al.,  
 207 2023; Kynkänniemi et al., 2024), which has shown promising results in DMs. Unlike dynamic CFG,  
 208 we aim to adjust  $w$  across layers rather than across time steps.

209 It is known that in transformer architectures, different layers are responsible for capturing semantics  
 210 at different levels (Avrahami et al., 2025). This motivates us to explore which layers are most suitable  
 211 for introducing guidance, depending on the targeted aspect.

212 Based on this, we propose applying dynamic modulation guidance at the layer level. We consider the  
 213 simplest variant present in Figure 3(b). We discuss more strategies in more detail in Appendix B.  
 214 First, we compare the dynamic version against constant modulation guidance in terms of the aesthetics–prompt  
 215 fidelity trade-off. To this end, we apply both types of guidance with different scales  $w$   
 216 on 1K prompts from the MJHQ dataset (Lian et al., 2023). We compute PickScore (Kirstain et al.,  
 217 2023) for aesthetics quality and CLIP score (Hessel et al., 2021) for text correspondence. The results  
 218 presented in Figure 3(a) confirm that dynamic guidance provides a better trade-off than constant  
 219 guidance. Our approach improves image quality without compromising prompt correspondence  
 220 relative to  $w = 0$  (the initial model without modulation guidance).

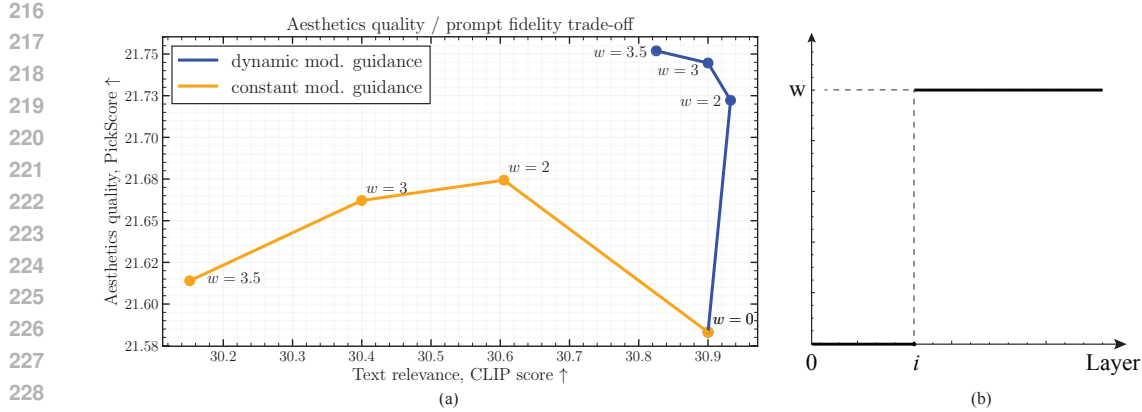


Figure 3: **Analysis on dynamic modulation guidance.** (a) Dynamic guidance offers a better trade-off between aesthetic quality and prompt correspondence than constant modulation guidance. (b) We use a step function, controlled by  $i$ , that skips the first few layers of the model as our form of dynamic guidance. Additional variants are explored in Appendix B.

Then, we compare the proposed dynamic guidance with constant guidance across different tasks, with results summarized in Table 7. We find that the simplest form of dynamic guidance performs strongly, outperforming the constant-scale baseline. Importantly, this strategy generalizes well across tasks, suggesting that it can be applied to new tasks without additional tuning. We also observe that more complex strategies can yield further improvements for `hands` correction, offering an extra degree of refinement for users who wish to build on top of the simplest method—an advantage that we believe is valuable in real-world applications.

#### What does modulation guidance actually do?

We address the question of how the model is affected by the guidance in improving the generated content. To this end, we analyze the case of `hands` correction. Specifically, in Figure 4(a), we visualize the attention map corresponding to the word `hands` for a specific image. Interestingly, we observe that the model places greater focus on the relevant region, highlighting it more distinctly. In addition, in Figure 4(b, left), we plot the averaged attention map for all tokens in the corresponding prompt. We find that the model primarily shifts its attention toward more relevant tokens—such as `hands` and `child`.

To confirm this intuition, we analyze a subset of prompts focused on `hands` correction and split all tokens into four groups: non-content tokens, the token `hands`, tokens related to `hands`, and other important tokens. The results in Figure 4(b, right) confirm that the model shifts its attention toward `hands` and hand-related tokens.

**Integrating the pooled text embedding into CLIP-free models.** Finally, we extend modulation guidance to models without pooled text embeddings, showing that it can improve generation quality. To this end, we fine-tune existing text-to-image/video models Agarwal et al. (2025); Wan et al. (2025) by introducing the pooled embedding. Specifically, we train a small MLP on top of the pooled text embedding and add it to the timestep embedding, while keeping the rest of the network frozen. The model behaves identically to the original when the pooled embedding is set to 0. Importantly, we train on the model’s own synthetic data to ensure that improvements do not stem from dataset differences.

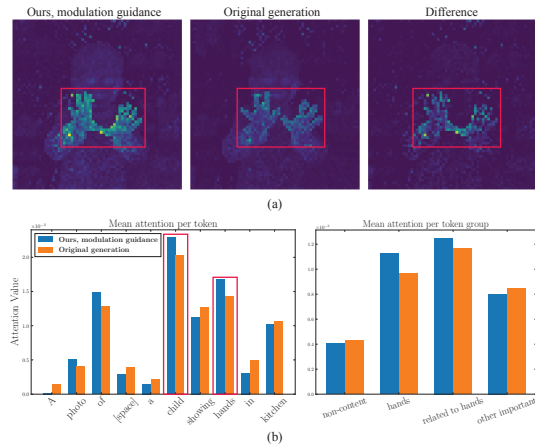


Figure 4: After applying modulation guidance, the model focuses more on the desired features, such as `hands` (a, b).

270  
 271 Table 2: Performance of text-to-image DMs with and without modulation guidance (gray)  
 272 on Aesthetics and Complexity, evaluated with human preferences and automatic metrics. Human  
 273 win rates are reported with respect to the original model; **green** indicates statistically significant  
 274 improvement, **red** a decline. For automatic metrics, **bold** denotes improvement over the original  
 275 model.

276 Model	277 Side-by-Side Win Rate, %				278 Automatic Metrics, COCO 5k			
	279 Relevance $\uparrow$	280 Aesthetics $\uparrow$	281 Complexity $\uparrow$	282 Defects $\uparrow$	283 PickScore $\uparrow$	284 CLIP $\uparrow$	285 IR $\uparrow$	286 HPSv3 $\uparrow$
<b>FLUX schnell</b>					22.9	35.6	10.2	11.3
Aesthetics	48	<b>72</b>	<b>78</b>	48	<b>23.1</b>	<b>35.8</b>	<b>11.0</b>	<b>11.8</b>
Complexity	53	<b>56</b>	<b>69</b>	47	<b>23.0</b>	<b>35.9</b>	<b>10.8</b>	<b>11.4</b>
<b>FLUX dev</b>					23.1	34.7	10.5	12.4
Aesthetics	<b>44</b>	<b>56</b>	<b>69</b>	52	<b>23.2</b>	34.5	<b>11.0</b>	<b>12.8</b>
Complexity	48	<b>59</b>	<b>72</b>	47	23.1	34.6	<b>11.1</b>	<b>12.8</b>
<b>SD3.5 Large</b>					23.0	35.8	10.5	11.1
Aesthetics	50	<b>62</b>	<b>70</b>	47	<b>23.1</b>	<b>35.9</b>	<b>10.7</b>	<b>11.2</b>
Complexity	49	49	<b>60</b>	45	23.0	35.8	<b>11.7</b>	11.0
<b>HiDream</b>					23.4	34.4	11.7	13.2
Aesthetics	49	<b>60</b>	<b>80</b>	46	<b>23.5</b>	34.4	<b>12.1</b>	<b>13.7</b>
Complexity	47	52	<b>70</b>	45	<b>23.5</b>	34.4	<b>11.9</b>	<b>13.3</b>
<b>COSMOS</b>					23.0	35.0	11.4	12.3
+ CLIP	50	49	<b>43</b>	50	23.0	35.0	11.4	12.2
Aesthetics	50	<b>60</b>	<b>70</b>	45	<b>23.2</b>	35.0	<b>11.7</b>	<b>12.6</b>
Complexity	50	52	<b>61</b>	<b>44</b>	23.0	<b>35.4</b>	<b>11.8</b>	<b>12.4</b>

291  
 292 We highlight two important aspects of the training process. First, we propagate the textual prompt  
 293 solely through the pooled text embedding, using an unconditional prompt for T5. This design forces  
 294 the model to perceive textual information through the pooled embedding. Second, we employ a  
 295 distillation-based training regime. Specifically, we sample a clean image, add noise to it, and then  
 296 generate two predictions: one from the original model (without the pooled embedding) and one from  
 297 the modified model (with the pooled embedding). The objective is to minimize the MSE loss between  
 298 these two predictions. This distillation approach is well-suited for few-step DMs, as it eliminates the  
 299 need for complex adversarial or distribution-matching losses (Yin et al., 2024a).

## 301 6 EXPERIMENTS

### 303 6.1 TEXT-TO-IMAGE GENERATION

305 **Configuration.** We validate our approach on state-of-the-art text-to-image DMs that include  
 306 modulation-based text conditioning: FLUX schnell (Sauer et al., 2024a), FLUX (Labs, 2024),  
 307 SD3.5 Large (Esser et al., 2024), and HiDream (Cai et al., 2025). In addition, we consider the  
 308 CLIP-free COSMOS model (Agarwal et al., 2025) and fine-tune it for 4K iterations to introduce the  
 309 pooled text embedding. We train the model on its own synthetic dataset of 500K samples, following  
 310 the generation settings of Agarwal et al. (2025) and using prompts from Li et al. (2024).

311 We evaluate performance using two types of metrics: human preference and automatic evaluation.  
 312 Human preference is measured via side-by-side comparisons, where annotators assess image pairs on  
 313 four criteria: text relevance, aesthetics, complexity, and defects (details in Appendix J). For general  
 314 changes, we use 128 prompts from PartiPrompts (Yu et al., 2022), generating two images per prompt.  
 315 For specific changes, we use 70 prompts from CompBench (Jia et al., 2025) for `object counting`  
 316 and 200 LLM-generated prompts for `hands correction`. For automatic evaluation, we report  
 317 CLIP score (Hessel et al., 2021), ImageReward (IR) (Xu et al., 2023), PickScore (PS) (Kirstain et al.,  
 318 2023), and HPSv3 (Ma et al., 2025b), tested on 5K prompts from COCO2014 (Lin et al., 2014). We  
 319 also use GenEval (Ghosh et al., 2023) to validate modulation guidance across multiple benchmark  
 320 criteria.

321 Our main baselines are the original models without modulation guidance. In addition, we con-  
 322 sider the Normalized Attention Guidance approach (Chen et al., 2025) and LLM-enhanced prompt  
 323 modifiers (Lian et al., 2023). Finally, we include the test-time optimization method Concept Slid-  
 324 ers (Gandikota et al., 2024) for the `hands correction` task.



Figure 5: Qualitative results of modulation guidance for Aesthetics (top) and Complexity (bottom). The Aesthetics guidance notably improves image quality, while the Complexity guidance can enhance the complexity of both the main object and background details.

**General changes.** In this case, we focus on two aspects for improvement: aesthetics and complexity. These aspects are crucial for text-to-image generation and are typically the targets of self-supervised fine-tuning techniques (Startsev et al., 2025) or RL-based approaches (Wallace et al., 2024), which are commonly adopted in DMs. However, we demonstrate that our simple technique achieves significant improvements without any fine-tuning. The only requirement is to select appropriate positive and negative prompts, along with a suitable dynamic guidance strategy. Our choices are summarized in Table 5 and discussed in Appendix D.

Table 2 reports numerical results, showing clear human preference gains for both aspects. Aesthetics guidance significantly improves both aesthetics and complexity, while complexity guidance mainly enhances complexity. Automatic metrics show consistent ImageReward gains across all models and HPSv3 improvements in most cases, except for SD3.5 Large with complexity guidance. Importantly, we observe that introducing CLIP into COSMOS does not improve performance and even reduces complexity; gains appear only when combined with modulation guidance, confirming that CLIP alone is ineffective. We note slight drops in text relevance for FLUX dev and in defects for COSMOS, though these are minor. Qualitative examples are shown in Figure 5 and Appendix I.

**Specific changes.** Next, we focus on improving object counting, hands correction, color, and position. The first two are particularly important, as they have been extensively studied in prior work (Binyamin et al., 2025; Gandikota et al., 2024). For object counting, we use the number of target objects as the positive direction, while for hands correction, we draw

378  
379 Table 3: Quantitative results of the modulation guidance for specific changes. The modulation  
380 guidance yields improvements according to GenEval and human preference.

381 <b>Model</b>		382 <b>GenEval</b>			383 <b>SbS Win Rate, %</b>	
		384 Object Counting	Color	Position	385 Object Counting	Hands correction
386 <b>FLUX schnell</b>	387 Original	388 56	389 79	390 25	391 39	392 41
	393 Ours	394 65 <b>(+9)</b>	395 86 <b>(+7)</b>	396 30 <b>(+5)</b>	397 61 <b>(+22)</b>	398 59 <b>(+18)</b>



414 Figure 6: Qualitative results of the modulation guidance for Object counting (top) and Hands  
415 correction (bottom).

416  
417 inspiration from Gandikota et al. (2024) in designing positive and negative prompts. Further details  
418 are provided in Table 5.

419  
420 We present the results in Table 3 and Figure 6. Improvements are observed in several aspects of the  
421 GenEval benchmark, including object counting, color, and position. According to human evaluation,  
422 our approach improves the original model by 22% in object counting and 18% in hands  
423 correction. We report text relevance and defects as the evaluation criteria for object counting  
424 and hands correction, respectively.

425 **Comparison with baselines.** Normalized Attention Guidance (Chen et al., 2025) targets general  
426 changes, so we compare it with our aesthetics guidance using SbS evaluation. Similarly, we  
427 compare Concept Sliders (Gandikota et al., 2024) with our hands correction guidance by  
428 evaluating defects. For LLM-enhanced prompts (Lian et al., 2023), we consider general changes,  
429 hands correction, and object counting. Results in Appendix E (Tables 8 and 9) show  
430 that our approach outperforms Normalized Attention Guidance by 34% and Concept Sliders by 16%,  
431 without additional computational overhead. Moreover, Table 8 shows that modulation guidance can  
further improve performance when combined with LLM-enhanced prompts.

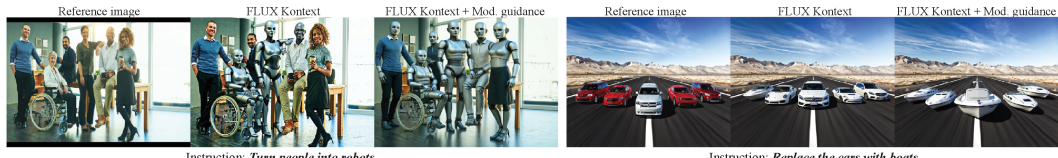
432 Table 4: Quantitative evaluation on VBench. The results show an improved dynamic degree compared  
 433 to the original models and baseline approach (normalized attention guidance).

434 Model, video	435	436 total score $\uparrow$	437 motion smoothness $\uparrow$	438 dynamic degree $\uparrow$	439 aesthetic quality $\uparrow$	440 overall consistency $\uparrow$
441 Hunyan, 13B	442 Original	443 56.68	444 <b>99.23</b>	445 50.51	446 55.88	447 21.08
	448 Modulation guidance	449 <b>57.56</b>	450 99.03	451 <b>53.61</b>	452 <b>56.50</b>	453 <b>21.09</b>
454 CausVid, 1.3B	455 Original	456 62.72	457 <b>98.76</b>	458 75.25	459 57.85	460 19.01
	461 + CLIP	462 62.82	463 98.63	464 76.38	465 57.77	466 18.49
	467 Norm. attent. guidance	468 63.58	469 98.39	470 74.22	471 <b>62.08</b>	472 <b>19.61</b>
473 Modulation guidance						
474						



475 *A bicycle gliding through a snowy field.*

476 Figure 7: Qualitative comparison between the original CausVid and CausVid with modulation  
 477 guidance.



478 Figure 8: Qualitative results for text-guided image editing tasks. We observe that FLUX Kontext  
 479 sometimes struggles with complex edits, while modulation guidance can mitigate this limitation.

## 480 6.2 TEXT-TO-VIDEO GENERATION

481 **Configuration.** We apply modulation guidance to Hunyan 13B (Kong et al., 2024) and CausVid  
 482 1.3B (Yin et al., 2024b). The latter does not include a CLIP model, so we fine-tune it for 1K iterations.  
 483 To evaluate performance, we use VBench (Huang et al., 2024), which covers various aspects. In this  
 484 experiment, we apply the same aesthetics guidance as in the text-to-image task. In addition, we  
 485 compare our approach with Normalized Attention Guidance.

486 **Results.** The results are presented in Table 4 and Figure 7. Importantly, we observe improvements in  
 487 dynamics for both models, with particularly strong gains for CausVid. This is notable because  
 488 CausVid is distilled from WAN (Wan et al., 2025), and video models typically lose dynamics after  
 489 distillation. Furthermore, we find that incorporating CLIP provides no improvement. Additional  
 490 visual comparisons are provided in Appendix I.

## 491 6.3 INSTRUCTION-GUIDED IMAGE EDITING

492 Finally, we address image editing using the FLUX Kontext model (Labs et al., 2025), which, as  
 493 we find, can struggle with complex edits involving multiple objects. To overcome this, we apply  
 494 modulation guidance, using the final prompt as the positive direction and a blank prompt as the  
 495 negative. We validate our approach on the SEED-Data benchmark (Ge et al., 2024) and present the  
 496 results and implementation details in Appendix F. Representative examples are shown in Figure 8.

## 497 7 CONCLUSION

498 In this paper, we revisit the role of the pooled text embedding, showing that, despite its weak influence,  
 499 it can improve performance across tasks and models when used from a different perspective. We  
 500 present ablation studies in Appendix C, where dynamic modulation guidance outperforms constant  
 501 guidance, offering greater flexibility for practitioners. Limitations are discussed in Appendix H.

486 REFERENCES  
487

488 Aishwarya Agarwal, Srikrishna Karanam, KJ Joseph, Apoorv Saxena, Koustava Goswami, and  
489 Balaji Vasan Srinivasan. A-star: Test-time attention segregation and retention for text-to-image  
490 synthesis. In *Proceedings of the IEEE/CVF International Conference on Computer Vision*, pp.  
491 2283–2293, 2023.

492 Niket Agarwal, Arslan Ali, Maciej Bala, Yogesh Balaji, Erik Barker, Tiffany Cai, Prithvijit Chat-  
493 topadhyay, Yongxin Chen, Yin Cui, Yifan Ding, et al. Cosmos world foundation model platform  
494 for physical ai. *arXiv preprint arXiv:2501.03575*, 2025.

495 Donghoon Ahn, Hyoungwon Cho, Jaewon Min, Wooseok Jang, Jungwoo Kim, SeonHwa Kim,  
496 Hyun Hee Park, Kyong Hwan Jin, and Seungryong Kim. Self-rectifying diffusion sampling with  
497 perturbed-attention guidance, 2025. URL <https://arxiv.org/abs/2403.17377>.

498 Omri Avrahami, Or Patashnik, Ohad Fried, Egor Nemchinov, Kfir Aberman, Dani Lischinski, and  
499 Daniel Cohen-Or. Stable flow: Vital layers for training-free image editing. In *Proceedings of the  
500 Computer Vision and Pattern Recognition Conference*, pp. 7877–7888, 2025.

501 Shuai Bai, Keqin Chen, Xuejing Liu, Jialin Wang, Wenbin Ge, Sibo Song, Kai Dang, Peng Wang,  
502 Shijie Wang, Jun Tang, Humen Zhong, Yuanzhi Zhu, Mingkun Yang, Zhaohai Li, Jianqiang Wan,  
503 Pengfei Wang, Wei Ding, Zheren Fu, Yiheng Xu, Jiabo Ye, Xi Zhang, Tianbao Xie, Zesen Cheng,  
504 Hang Zhang, Zhibo Yang, Haiyang Xu, and Junyang Lin. Qwen2.5-v1 technical report. *arXiv  
505 preprint arXiv:2502.13923*, 2025.

506 Lital Binyamin, Yoad Tewel, Hilit Segev, Eran Hirsch, Royi Rassin, and Gal Chechik. Make it count:  
507 Text-to-image generation with an accurate number of objects. In *Proceedings of the Computer  
508 Vision and Pattern Recognition Conference*, pp. 13242–13251, 2025.

509 Qi Cai, Jingwen Chen, Yang Chen, Yehao Li, Fuchen Long, Yingwei Pan, Zhaofan Qiu, Yiheng  
510 Zhang, Fengbin Gao, Peihan Xu, et al. Hidream-i1: A high-efficient image generative foundation  
511 model with sparse diffusion transformer. *arXiv preprint arXiv:2505.22705*, 2025.

512 Hila Chefer, Yuval Alaluf, Yael Vinker, Lior Wolf, and Daniel Cohen-Or. Attend-and-excite:  
513 Attention-based semantic guidance for text-to-image diffusion models. *ACM transactions on  
514 Graphics (TOG)*, 42(4):1–10, 2023.

515 Dar-Yen Chen, Hmrishav Bandyopadhyay, Kai Zou, and Yi-Zhe Song. Normalized attention guidance:  
516 Universal negative guidance for diffusion models, 2025. URL <https://arxiv.org/abs/2505.21179>.

517 Minghao Chen, Iro Laina, and Andrea Vedaldi. Training-free layout control with cross-attention  
518 guidance. In *Proceedings of the IEEE/CVF winter conference on applications of computer vision*,  
519 pp. 5343–5353, 2024.

520 Hyungjin Chung, Jeongsol Kim, Geon Yeong Park, Hyelin Nam, and Jong Chul Ye. Cfg++: Manifold-  
521 constrained classifier free guidance for diffusion models. *arXiv preprint arXiv:2406.08070*, 2024.

522 Omer Dahary, Or Patashnik, Kfir Aberman, and Daniel Cohen-Or. Be yourself: Bounded attention  
523 for multi-subject text-to-image generation, 2024. URL <https://arxiv.org/abs/2403.16990>.

524 Yusuf Dalva, Kavana Venkatesh, and Pinar Yanardag. Fluxspace: Disentangled semantic editing in  
525 rectified flow transformers, 2024. URL <https://arxiv.org/abs/2412.09611>.

526 Patrick Esser, Sumith Kulal, Andreas Blattmann, Rahim Entezari, Jonas Müller, Harry Saini, Yam  
527 Levi, Dominik Lorenz, Axel Sauer, Frederic Boesel, et al. Scaling rectified flow transformers for  
528 high-resolution image synthesis. In *Forty-first international conference on machine learning*, 2024.

529 Luca Eyring, Shyamgopal Karthik, Karsten Roth, Alexey Dosovitskiy, and Zeynep Akata. Reno:  
530 Enhancing one-step text-to-image models through reward-based noise optimization. *Neural  
531 Information Processing Systems (NeurIPS)*, 2024.

540 Luca Eyring, Shyamgopal Karthik, Alexey Dosovitskiy, Nataniel Ruiz, and Zeynep Akata. Noise hy-  
 541 pernetworks: Amortizing test-time compute in diffusion models. *arXiv preprint arXiv:2508.09968*,  
 542 2025.

543 Weichen Fan, Amber Yijia Zheng, Raymond A Yeh, and Ziwei Liu. Cfg-zero\*: Improved classifier-  
 544 free guidance for flow matching models. *arXiv preprint arXiv:2503.18886*, 2025.

545 Rohit Gandikota, Joanna Materzyńska, Tingrui Zhou, Antonio Torralba, and David Bau. Concept  
 546 sliders: Lora adaptors for precise control in diffusion models. In *European Conference on Computer  
 547 Vision*, pp. 172–188. Springer, 2024.

548 Rohit Gandikota, Zongze Wu, Richard Zhang, David Bau, Eli Shechtman, and Nick Kolkin. Slider-  
 549 space: Decomposing the visual capabilities of diffusion models. *arXiv preprint arXiv:2502.01639*,  
 550 2025.

551 Daniel Garibi, Shahar Yadin, Roni Paiss, Omer Tov, Shiran Zada, Ariel Ephrat, Tomer Michaeli, Inbar  
 552 Mosseri, and Tali Dekel. Tokenverse: Versatile multi-concept personalization in token modulation  
 553 space, 2025. URL <https://arxiv.org/abs/2501.12224>.

554 Yuying Ge, Sijie Zhao, Chen Li, Yixiao Ge, and Ying Shan. Seed-data-edit technical report: A  
 555 hybrid dataset for instructional image editing, 2024. URL <https://arxiv.org/abs/2405.04007>.

556 Dhruba Ghosh, Hannaneh Hajishirzi, and Ludwig Schmidt. Geneval: An object-focused framework  
 557 for evaluating text-to-image alignment. *Advances in Neural Information Processing Systems*, 36:  
 558 52132–52152, 2023.

559 Xiefan Guo, Jinlin Liu, Miaomiao Cui, Jiankai Li, Hongyu Yang, and Di Huang. Initno: Boosting  
 560 text-to-image diffusion models via initial noise optimization, 2024. URL <https://arxiv.org/abs/2404.04650>.

561 Jack Hessel, Ari Holtzman, Maxwell Forbes, Ronan Le Bras, and Yejin Choi. Clipscore: A reference-  
 562 free evaluation metric for image captioning. *arXiv preprint arXiv:2104.08718*, 2021.

563 Jonathan Ho and Tim Salimans. Classifier-free diffusion guidance. *arXiv preprint arXiv:2207.12598*,  
 564 2022.

565 Jonathan Ho, Ajay Jain, and Pieter Abbeel. Denoising diffusion probabilistic models. *Advances in  
 566 neural information processing systems*, 33:6840–6851, 2020.

567 Susung Hong, Gyuseong Lee, Wooseok Jang, and Seungryong Kim. Improving sample quality  
 568 of diffusion models using self-attention guidance, 2023. URL <https://arxiv.org/abs/2210.00939>.

569 Ziqi Huang, Yinan He, Jiashuo Yu, Fan Zhang, Chenyang Si, Yuming Jiang, Yuanhan Zhang, Tianxing  
 570 Wu, Qingyang Jin, Nattapol Champaosit, Yaohui Wang, Xinyuan Chen, Limin Wang, Dahua Lin,  
 571 Yu Qiao, and Ziwei Liu. VBench: Comprehensive benchmark suite for video generative models.  
 572 In *Proceedings of the IEEE/CVF Conference on Computer Vision and Pattern Recognition*, 2024.

573 Bohan Jia, Wenxuan Huang, Yuntian Tang, Junbo Qiao, Jincheng Liao, Shaosheng Cao, Fei Zhao,  
 574 Zhaopeng Feng, Zhouhong Gu, Zhenfei Yin, Lei Bai, Wanli Ouyang, Lin Chen, Fei Zhao, Zihan  
 575 Wang, Yuan Xie, and Shaohui Lin. Compbench: Benchmarking complex instruction-guided image  
 576 editing, 2025. URL <https://arxiv.org/abs/2505.12200>.

577 Tero Karras, Timo Aila, Samuli Laine, and Jaakko Lehtinen. Progressive growing of gans for  
 578 improved quality, stability, and variation. *arXiv preprint arXiv:1710.10196*, 2017.

579 Tero Karras, Samuli Laine, and Timo Aila. A style-based generator architecture for generative  
 580 adversarial networks. In *Proceedings of the IEEE/CVF conference on computer vision and pattern  
 581 recognition*, pp. 4401–4410, 2019.

582 Tero Karras, Miika Aittala, Janne Hellsten, Samuli Laine, Jaakko Lehtinen, and Timo Aila. Training  
 583 generative adversarial networks with limited data. In *Proc. NeurIPS*, 2020.

594 Tero Karras, Miika Aittala, Samuli Laine, Erik Härkönen, Janne Hellsten, Jaakko Lehtinen, and Timo  
 595 Aila. Alias-free generative adversarial networks. In *Proc. NeurIPS*, 2021.  
 596

597 Tero Karras, Miika Aittala, Tuomas Kynkänniemi, Jaakko Lehtinen, Timo Aila, and Samuli Laine.  
 598 Guiding a diffusion model with a bad version of itself. *Advances in Neural Information Processing  
 599 Systems*, 37:52996–53021, 2024.

600 Yuval Kirstain, Adam Polyak, Uriel Singer, Shahbuland Matiana, Joe Penna, and Omer Levy. Pick-  
 601 a-pic: An open dataset of user preferences for text-to-image generation. *Advances in neural  
 602 information processing systems*, 36:36652–36663, 2023.  
 603

604 Weijie Kong, Qi Tian, Zijian Zhang, Rox Min, Zuozhuo Dai, Jin Zhou, Jiangfeng Xiong, Xin Li,  
 605 Bo Wu, Jianwei Zhang, et al. Hunyuandvideo: A systematic framework for large video generative  
 606 models. *arXiv preprint arXiv:2412.03603*, 2024.

607 Mingi Kwon, Jaeseok Jeong, and Youngjung Uh. Diffusion models already have a semantic latent  
 608 space. *arXiv preprint arXiv:2210.10960*, 2022.  
 609

610 Tuomas Kynkänniemi, Miika Aittala, Tero Karras, Samuli Laine, Timo Aila, and Jaakko Lehtinen.  
 611 Applying guidance in a limited interval improves sample and distribution quality in diffusion  
 612 models. *Advances in Neural Information Processing Systems*, 37:122458–122483, 2024.

613 Black Forest Labs. Flux. <https://github.com/black-forest-labs/flux>, 2024.  
 614

615 Black Forest Labs, Stephen Batifol, Andreas Blattmann, Frederic Boesel, Saksham Consul, Cyril  
 616 Diagne, Tim Dockhorn, Jack English, Zion English, Patrick Esser, Sumith Kulal, Kyle Lacey, Yam  
 617 Levi, Cheng Li, Dominik Lorenz, Jonas Müller, Dustin Podell, Robin Rombach, Harry Saini, Axel  
 618 Sauer, and Luke Smith. Flux.1 kontext: Flow matching for in-context image generation and editing  
 619 in latent space, 2025. URL <https://arxiv.org/abs/2506.15742>.

620 Daiqing Li, Aleks Kamko, Ehsan Akhgari, Ali Sabet, Linmiao Xu, and Suhail Doshi. Playground  
 621 v2.5: Three insights towards enhancing aesthetic quality in text-to-image generation, 2024.  
 622

623 Yumeng Li, Margret Keuper, Dan Zhang, and Anna Khoreva. Divide & bind your attention for  
 624 improved generative semantic nursing. *arXiv preprint arXiv:2307.10864*, 2023.  
 625

626 Long Lian, Boyi Li, Adam Yala, and Trevor Darrell. Llm-grounded diffusion: Enhancing prompt  
 627 understanding of text-to-image diffusion models with large language models. *arXiv preprint  
 628 arXiv:2305.13655*, 2023.

629 Shanchuan Lin, Bingchen Liu, Jiashi Li, and Xiao Yang. Common diffusion noise schedules and  
 630 sample steps are flawed. In *Proceedings of the IEEE/CVF winter conference on applications of  
 631 computer vision*, pp. 5404–5411, 2024.  
 632

633 Tsung-Yi Lin, Michael Maire, Serge Belongie, James Hays, Pietro Perona, Deva Ramanan, Piotr  
 634 Dollár, and C Lawrence Zitnick. Microsoft coco: Common objects in context. In *European  
 635 conference on computer vision*, pp. 740–755. Springer, 2014.

636 Nanye Ma, Shangyuan Tong, Haolin Jia, Hexiang Hu, Yu-Chuan Su, Mingda Zhang, Xuan Yang,  
 637 Yandong Li, Tommi Jaakkola, Xuhui Jia, et al. Inference-time scaling for diffusion models beyond  
 638 scaling denoising steps. *arXiv preprint arXiv:2501.09732*, 2025a.  
 639

640 Yuhang Ma, Xiaoshi Wu, Keqiang Sun, and Hongsheng Li. Hpsv3: Towards wide-spectrum human  
 641 preference score. *arXiv preprint arXiv:2508.03789*, 2025b.  
 642

643 Arash Marioriyad, Mohammadali Banayeeanzade, Reza Abbasi, Mohammad Hossein Rohban, and  
 644 Mahdieh Soleymani Baghshah. Attention overlap is responsible for the entity missing problem in  
 645 text-to-image diffusion models!, 2025. URL <https://arxiv.org/abs/2410.20972>.

646 Viet Nguyen, Anh Nguyen, Trung Dao, Khoi Nguyen, Cuong Pham, Toan Tran, and Anh Tran.  
 647 Snoopi: Supercharged one-step diffusion distillation with proper guidance, 2024. URL <https://arxiv.org/abs/2412.02687>.

648 Alex Nichol, Prafulla Dhariwal, Aditya Ramesh, Pranav Shyam, Pamela Mishkin, Bob McGrew,  
 649 Ilya Sutskever, and Mark Chen. Glide: Towards photorealistic image generation and editing with  
 650 text-guided diffusion models. *arXiv preprint arXiv:2112.10741*, 2021.

651

652 Jonas Oppenlaender. A taxonomy of prompt modifiers for text-to-image generation. *Behaviour &*  
 653 *Information Technology*, 43(15):3763–3776, 2024.

654

655 William Peebles and Saining Xie. Scalable diffusion models with transformers. In *Proceedings of*  
 656 *the IEEE/CVF international conference on computer vision*, pp. 4195–4205, 2023.

657

658 Quynh Phung, Songwei Ge, and Jia-Bin Huang. Grounded text-to-image synthesis with attention refo-  
 659 cusing. In *Proceedings of the IEEE/CVF Conference on Computer Vision and Pattern Recognition*,  
 660 pp. 7932–7942, 2024.

661

662 Dustin Podell, Zion English, Kyle Lacey, Andreas Blattmann, Tim Dockhorn, Jonas Müller, Joe  
 663 Penna, and Robin Rombach. Sdxl: Improving latent diffusion models for high-resolution image  
 664 synthesis. *arXiv preprint arXiv:2307.01952*, 2023.

665

666 Alec Radford, Jong Wook Kim, Chris Hallacy, Aditya Ramesh, Gabriel Goh, Sandhini Agarwal,  
 667 Girish Sastry, Amanda Askell, Pamela Mishkin, Jack Clark, et al. Learning transferable visual  
 668 models from natural language supervision. In *International conference on machine learning*, pp.  
 669 8748–8763. PMLR, 2021.

670

671 Colin Raffel, Noam Shazeer, Adam Roberts, Katherine Lee, Sharan Narang, Michael Matena, Yanqi  
 672 Zhou, Wei Li, and Peter J Liu. Exploring the limits of transfer learning with a unified text-to-text  
 673 transformer. *Journal of machine learning research*, 21(140):1–67, 2020.

674

675 Aditya Ramesh, Prafulla Dhariwal, Alex Nichol, Casey Chu, and Mark Chen. Hierarchical text-  
 676 conditional image generation with clip latents. *arXiv preprint arXiv:2204.06125*, 1(2):3, 2022.

677

678 Royi Rassin, Eran Hirsch, Daniel Glickman, Shauli Ravfogel, Yoav Goldberg, and Gal Chechik.  
 679 Linguistic binding in diffusion models: Enhancing attribute correspondence through attention map  
 680 alignment. *Advances in Neural Information Processing Systems*, 36:3536–3559, 2023.

681

682 Robin Rombach, Andreas Blattmann, Dominik Lorenz, Patrick Esser, and Björn Ommer. High-  
 683 resolution image synthesis with latent diffusion models. In *Proceedings of the IEEE/CVF confer-  
 684 ence on computer vision and pattern recognition*, pp. 10684–10695, 2022.

685

686 Olaf Ronneberger, Philipp Fischer, and Thomas Brox. U-net: Convolutional networks for biomedical  
 687 image segmentation. In *International Conference on Medical image computing and computer-  
 688 assisted intervention*, pp. 234–241. Springer, 2015.

689

690 Seyedmorteza Sadat, Jakob Buhmann, Derek Bradley, Otmar Hilliges, and Romann M Weber. Cads:  
 691 Unleashing the diversity of diffusion models through condition-annealed sampling. *arXiv preprint*  
 692 *arXiv:2310.17347*, 2023.

693

694 Seyedmorteza Sadat, Otmar Hilliges, and Romann M Weber. Eliminating oversaturation and artifacts  
 695 of high guidance scales in diffusion models. In *The Thirteenth International Conference on*  
 696 *Learning Representations*, 2024.

697

698 Seyedmorteza Sadat, Tobias Vontobel, Farnood Salehi, and Romann M Weber. Guidance in the fre-  
 699 quency domain enables high-fidelity sampling at low cfg scales. *arXiv preprint arXiv:2506.19713*,  
 700 2025.

701

702 Chitwan Saharia, William Chan, Saurabh Saxena, Lala Li, Jay Whang, Emily L Denton, Kamyar  
 703 Ghasemipour, Raphael Gontijo Lopes, Burcu Karagol Ayan, Tim Salimans, et al. Photorealistic  
 704 text-to-image diffusion models with deep language understanding. *Advances in neural information*  
 705 *processing systems*, 35:36479–36494, 2022.

706

707 Axel Sauer, Frederic Boesel, Tim Dockhorn, Andreas Blattmann, Patrick Esser, and Robin Rombach.  
 708 Fast high-resolution image synthesis with latent adversarial diffusion distillation. In *SIGGRAPH*  
 709 *Asia 2024 Conference Papers*, pp. 1–11, 2024a.

702 Axel Sauer, Dominik Lorenz, Andreas Blattmann, and Robin Rombach. Adversarial diffusion  
 703 distillation. In *European Conference on Computer Vision*, pp. 87–103. Springer, 2024b.  
 704

705 Hoigi Seo, Junseo Bang, Haechang Lee, Joohoon Lee, Byung Hyun Lee, and Se Young Chun.  
 706 Geometrical properties of text token embeddings for strong semantic binding in text-to-image  
 707 generation. *arXiv preprint arXiv:2503.23011*, 2025.

708 Yang Song, Jascha Sohl-Dickstein, Diederik P Kingma, Abhishek Kumar, Stefano Ermon, and Ben  
 709 Poole. Score-based generative modeling through stochastic differential equations. *arXiv preprint*  
 710 *arXiv:2011.13456*, 2020.

711 Yang Song, Prafulla Dhariwal, Mark Chen, and Ilya Sutskever. Consistency models. 2023.  
 712

713 Nikita Starodubcev, Denis Kuznedelev, Artem Babenko, and Dmitry Baranchuk. Scale-wise distilla-  
 714 tion of diffusion models. *arXiv preprint arXiv:2503.16397*, 2025.

715 Valerii Startsev, Alexander Ustyuzhanin, Alexey Kirillov, Dmitry Baranchuk, and Sergey Kas-  
 716 tryulin. Alchemist: Turning public text-to-image data into generative gold. *arXiv preprint*  
 717 *arXiv:2505.19297*, 2025.

718 Ashish Vaswani, Noam Shazeer, Niki Parmar, Jakob Uszkoreit, Llion Jones, Aidan N Gomez, Łukasz  
 719 Kaiser, and Illia Polosukhin. Attention is all you need. *Advances in neural information processing*  
 720 *systems*, 30, 2017.

721 Bram Wallace, Meihua Dang, Rafael Rafailev, Linqi Zhou, Aaron Lou, Senthil Purushwalkam,  
 722 Stefano Ermon, Caiming Xiong, Shafiq Joty, and Nikhil Naik. Diffusion model alignment using  
 723 direct preference optimization. In *Proceedings of the IEEE/CVF Conference on Computer Vision*  
 724 *and Pattern Recognition*, pp. 8228–8238, 2024.

725

726 Team Wan, Ang Wang, Baole Ai, Bin Wen, Chaojie Mao, Chen-Wei Xie, Di Chen, Feiwu Yu,  
 727 Haiming Zhao, Jianxiao Yang, et al. Wan: Open and advanced large-scale video generative models.  
 728 *arXiv preprint arXiv:2503.20314*, 2025.

729

730 Xi Wang, Nicolas Dufour, Nefeli Andreou, Marie-Paule Cani, Victoria Fernández Abrevaya, David  
 731 Picard, and Vicky Kalogeiton. Analysis of classifier-free guidance weight schedulers. *arXiv*  
 732 *preprint arXiv:2404.13040*, 2024.

733

734 Chenfei Wu, Jiahao Li, Jingren Zhou, Junyang Lin, Kaiyuan Gao, Kun Yan, Sheng-ming Yin, Shuai  
 735 Bai, Xiao Xu, Yilei Chen, et al. Qwen-image technical report. *arXiv preprint arXiv:2508.02324*,  
 2025.

736

737 Enze Xie, Junsong Chen, Junyu Chen, Han Cai, Haotian Tang, Yujun Lin, Zhekai Zhang, Muyang Li,  
 738 Ligeng Zhu, Yao Lu, et al. Sana: Efficient high-resolution image synthesis with linear diffusion  
 739 transformers. *arXiv preprint arXiv:2410.10629*, 2024.

740

741 Jiazheng Xu, Xiao Liu, Yuchen Wu, Yuxuan Tong, Qinkai Li, Ming Ding, Jie Tang, and Yuxiao Dong.  
 742 Imagereward: Learning and evaluating human preferences for text-to-image generation. *Advances*  
 743 *in Neural Information Processing Systems*, 36:15903–15935, 2023.

744

745 Shai Yehezkel, Omer Dahary, Andrey Voynov, and Daniel Cohen-Or. Navigating with annealing  
 746 guidance scale in diffusion space. *arXiv preprint arXiv:2506.24108*, 2025.

747

748 Sapir Esther Yiflach, Yuval Atzmon, and Gal Chechik. Data-driven loss functions for inference-time  
 749 optimization in text-to-image generation. *arXiv preprint arXiv:2509.02295*, 2025.

750

751 Tianwei Yin, Michaël Gharbi, Taesung Park, Richard Zhang, Eli Shechtman, Fredo Durand, and Bill  
 752 Freeman. Improved distribution matching distillation for fast image synthesis. *Advances in neural*  
 753 *information processing systems*, 37:47455–47487, 2024a.

754

755 Tianwei Yin, Qiang Zhang, Richard Zhang, William T Freeman, Fredo Durand, Eli Shechtman,  
 756 and Xun Huang. From slow bidirectional to fast causal video generators. *arXiv e-prints*, pp.  
 757 arXiv–2412, 2024b.

758

759 Jiahui Yu, Yuanzhong Xu, Jing Yu Koh, Thang Luong, Gunjan Baid, Zirui Wang, Vijay Vasudevan,  
 760 Alexander Ku, Yinfei Yang, Burcu Karagol Ayan, et al. Scaling autoregressive models for content-  
 761 rich text-to-image generation. *arXiv preprint arXiv:2206.10789*, 2(3):5, 2022.



756  
757  
758  
759  
760  
761  
762  
763  
764  
765  
766  
767  
768  
769  
770  
771  
772  
773  
774  
775  
776  
777  
778  
779  
780  
781  
782  
783  
784  
785  
786  
787  
788  
789  
790  
791  
792  
793  
794  
795  
796  
797  
798  
799  
800  
801  
802  
803  
804  
805  
806  
807  
808  
809

Figure 9: We observe that the CLIP text encoder does not influence instruction-guided image editing performed with the FLUX kontext model.

Table 5: Configuration of hyperparameters for dynamic modulation guidance

Task	Positive prompt	Negative prompt	Guidance strategy
Text-to-image aesthetics	Ultra-detailed, photorealistic, cinematic	Low-res, flat, cartoonish	Strategy 1 in Figure 3(b) $i = 5, w = 3$
Text-to-image complexity	Extremely complex, the highest quality	Very simple, no details at all	Strategy 1 in Figure 3(b) $i = 10, w = 3$
Text-to-image hands correction	Natural and realistic hands	Unnatural hands	Strategy 4 in Figure 3(b) $i_1 = 13, i_2 = 30, i_3 = 45$ $w_1 = 3, w_2 = 1$
Text-to-image object counting	[ $n$ ] [objects]	Very simple, no details at all	Strategy 1 in Figure 3(b) $i = 5, w = 3$
Text-to-video	Ultra-detailed, photorealistic, cinematic	Low-res, flat, cartoonish	Strategy 1 in Figure 3(b) $i = 5, w = 3$
Image editing	Textual prompt	—	Strategy 1 in Figure 3(b) $i = 5, w = 3$

## APPENDIX

### A ADDITIONAL ANALYSIS FOR FLUX KONTEXT MODEL

Here, we analyze the impact of the CLIP model on FLUX Kontext (Labs et al., 2025). We find that dropping the pooled embedding does not affect editing results, as visually confirmed in Figure 9. In addition, we evaluate performance on the SEED-Data benchmark (Ge et al., 2024) with and without the pooled text embedding. We compute the CLIP score (Hessel et al., 2021) to measure reference preservation and prompt correspondence. The results in Table 6 confirm the observation.

Table 6: Editing quality for the FLUX kontext model (with and without CLIP). CLIP has no effect on the model.

Configuration	CLIP Score, Image $\uparrow$	CLIP Score, Text $\uparrow$
CLIP+T5	79.3	29.3
w/o CLIP	80 (+0.7)	29.3 (0)

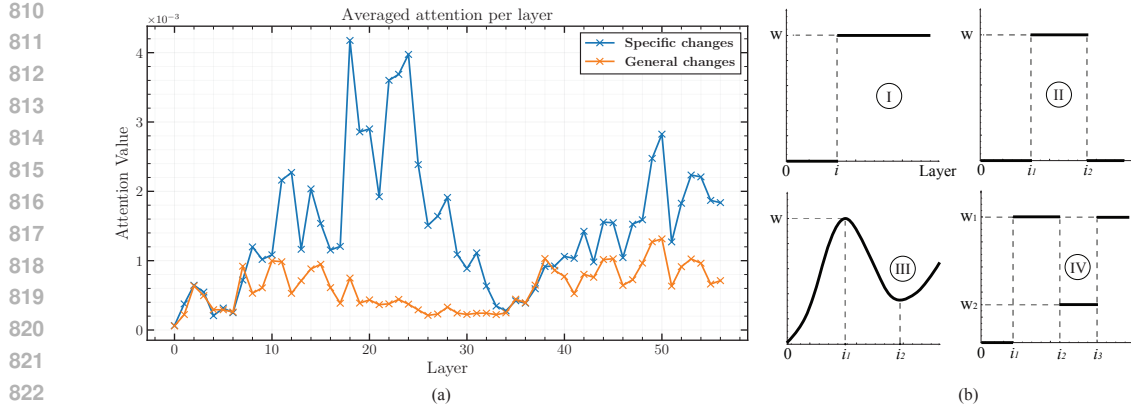


Figure 10: **Analysis on dynamic modulation guidance.** To derive a dynamic guidance scale, we (a) analyze how the model allocates attention to different features by computing averaged attention maps over two token groups (specific and general). Building on this, we (b) explore dynamic strategies for setting layer-specific  $w$  values.

The lack of impact in the editing case may stem from the out-of-distribution nature of instructions for the CLIP model. We find that this mismatch can lead to a lack of editing strength, particularly in complex scenes with multiple objects. To address this, we propose using the final prompt as the CLIP input and applying modulation guidance.

## B STRATEGIES FOR DYNAMIC GUIDANCE

Recent studies show that attention layers in transformer models specialize at different depths, with each layer focusing on distinct levels of semantic detail (Avrahami et al., 2025). This insight encourages us to investigate which parts of the attention stack are most appropriate for injecting guidance, depending on the desired effect. For example, if fine-grained attributes such as hands are mainly shaped by mid-layer attention, then targeting guidance at those specific layers is more effective and reduces the risk of unintended modifications in other regions of the image.

Thus, we construct two prompt subsets of 1,000 examples each: one targeting local features (e.g., hands, face, eyes) and the other targeting global features (e.g., realism, cinematic, crisp). We then generate images for each subset and collect the corresponding attention maps for each target aspect. Finally, we average these maps across all examples and present the results for different layers in Figure 10(a). We observe that the model primarily focuses on local features in two layer regions: layers 10–30 and 42–58. In contrast, attention to global features remains relatively constant, with a slight drop between layers 20 and 35.

Based on this analysis, we propose applying dynamic modulation guidance at the layer level. We present four possible strategies in Figure 10(b), with strategies 3 and 4 designed to resemble the observed attention behavior for specific changes. Interestingly, in Appendix C, we find that these strategies provide better results for hands correction. For global changes, the step function (case 1) performs well, outperforming the constant scale. Despite introducing additional hyperparameters, our dynamic guidance offers an extra degree of improvement for practitioners, which we believe is important in real-world applications.

## C ABLATION STUDY

**Dynamic modulation guidance.** First, we ablate different dynamic modulation guidance strategies. Specifically, we consider the FLUX schnell model, testing it on the aesthetics, hands correction, and object counting aspects.

We consider different dynamic guidance strategies from Figure 10(b) and compare them to a constant value of  $w = 3$ . For dynamic strategies, we use the following parameters.

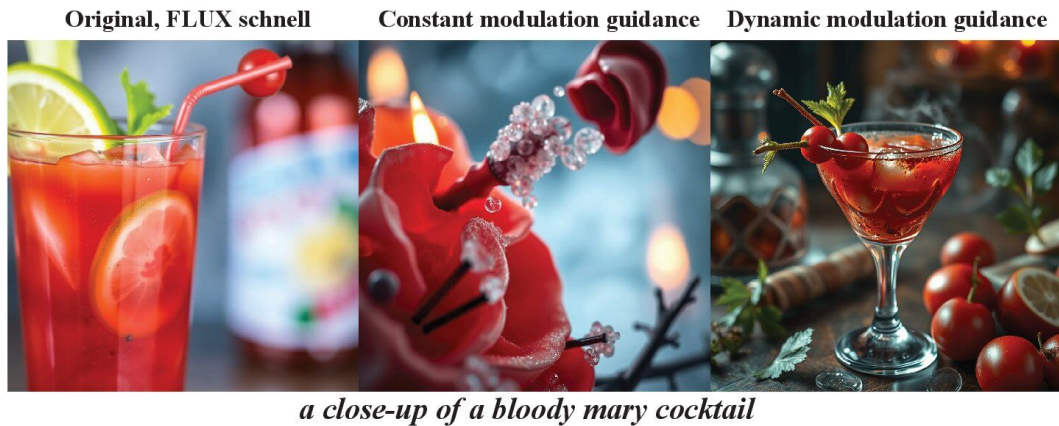
864

865  
866  
867  
Table 7: Ablation study of dynamic modulation guidance strategies using human preference (side-  
by-side win rate). The results demonstrate that dynamic guidance outperforms a constant guidance  
approach.

Configuration		Constant	Strategy 1	Strategy 2	Strategy 3	Strategy 4
Hands correction	Original	52	48	49	45	41
	Ours	48 <b>(-4)</b>	52 <b>(+4)</b>	51 <b>(+2)</b>	55 <b>(+10)</b>	59 <b>(+18)</b>
Object counting	Original	50	39	40	45	39
	Ours	50 <b>(-0)</b>	61 <b>(+22)</b>	60 <b>(+20)</b>	55 <b>(+10)</b>	61 <b>(+22)</b>
Aesthetics	Original	38	28	43	43	46
	Ours	62 <b>(+24)</b>	72 <b>(+44)</b>	57 <b>(+14)</b>	57 <b>(+14)</b>	54 <b>(+8)</b>

876

877

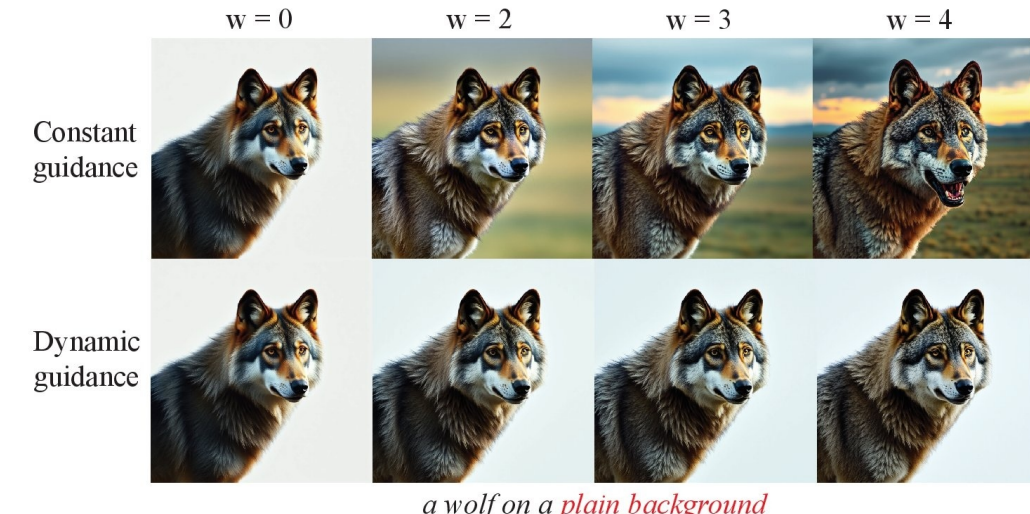


891

892  
893  
894  
895  
Figure 11: Qualitative comparison of modulation strategies for aesthetics. Constant guidance can  
overweight the original prompt, leading to significant divergence, whereas dynamic guidance better  
balances quality and prompt correspondence, allowing the use of larger  $w$  without degradation.

896

897



913

914

915  
916  
917  
Figure 12: We find that dynamic modulation guidance improves image content (e.g., makes the wolf's  
fur more detailed) while preserving prompt correspondence. In contrast, constant scales can neglect  
the prompt request even at small scales ( $w=2$ ).



Imagine a meticulously detailed, hyperrealistic portrait of an aged sage with piercing eyes and a flowing, white beard ...

Figure 13: Influence of starting layers for complexity guidance. Different choices of  $i$  with fixed  $w = 3$  illustrate how earlier or later starting layers balance between preserving the original image and improving complexity. In particular,  $i = 18$  and  $i = 28$  preserve the overall image while enhancing fine-grained details such as faces and hands.

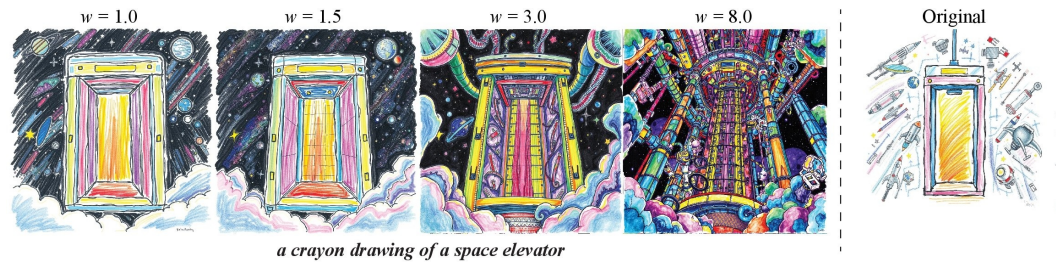


Figure 14: Influence of guidance strength  $w$  for aesthetics. With fixed  $i = 5$ , increasing  $w$  improves image quality by boosting the main object (the elevator) and background details. However, excessively large values, such as  $w = 8.0$ , can introduce artifacts.

- **Strategy 1.**  $i = 5, w = 3$ ;
- **Strategy 2.**  $i_1 = 13, i_2 = 30, w = 3$ ;
- **Strategy 3.** We use two exponential functions with centers at  $i_1 = 20, i_2 = 50$ , and  $w = 3$ ;
- **Strategy 4.**  $i_1 = 13, i_2 = 30, i_3 = 45, w_1 = 3, w_2 = 1$ .

Strategies 3 and 4 are designed to follow the attention pattern illustrated in Figure 10(a).

We conduct a human preference study comparing these strategies to the original model, with results presented in Table 7. First, we observe that dynamic strategies yield higher performance gains compared to a constant scale for hands correction and object counting. Moreover, strategy 4 demonstrates the best performance on hands correction, which aligns with the analysis of attention behavior. For object counting, strategies 1 and 4 perform equally well. We therefore select strategy 1 for this aspect due to its simplicity.

Second, for aesthetics guidance, we observe that strategy 1 achieves the best results, while constant guidance also performs well. However, we find that a constant  $w$  can introduce artifacts. As shown in Figure 11, constant guidance can overweight the original prompt, causing significant divergence from the source image. **In contrast, dynamic guidance achieves a better balance between quality enhancement and prompt correspondence, enabling the use of higher  $w$  values without introducing artifacts as shown in Figure 12.**

**Influence of guidance strength and starting layer number.** Next, we analyze how the results change across different starting layers  $i$  and modulation guidance strengths  $w$ . Our main dynamic strategy is the step function (strategy 1 in Figure 3b), and we ablate different choices for this strategy.

972  
973  
974  
975  
976  
977  
978  
979  
980  
981  
982  
983  
984  
985  
986  
987  
988  
989  
990  
991  
992  
993

**w = 0**  
**w = 3**



*a close-up of an old-fashioned cocktail*

994  
995  
996 Figure 15: We apply modulation guidance across different CFG values and observe consistent  
997 improvements, confirming that it is complementary to CFG.  
998  
999

1000 Specifically, in Figure 13, we evaluate different starting layers  $i$  with a fixed  $w = 3$  under complexity  
1001 guidance. This setting allows us to balance original image preservation with complexity improvement.  
1002 In particular,  $i = 18$  and  $i = 28$  fully preserve the original image while enhancing only fine-grained  
1003 details such as face and hands.

1004 Then, in Figure 14, we examine the influence of different  $w$  values with a fixed starting layer  $i = 5$   
1005 under aesthetics guidance. We observe that higher  $w$  enhances the main object (e.g., the *elevator*  
1006 in the example) but also improves background details. However, excessively large values, such as  
1007  $w = 8$ , may introduce artifacts.

1008 **Modulation guidance for different CFG.** Finally, we examine how modulation guidance behaves  
1009 under different CFG values, demonstrating that it can operate effectively on top of CFG. Using the  
1010 FLUX dev model with complexity guidance, we evaluate multiple CFG values in combination with  
1011 modulation guidance. The results in Figure 15 show that modulation guidance improves performance  
1012 across different CFG values, confirming that it is complementary to CFG.

## 1015 D HYPERPARAMETERS CHOICE

1016  
1017 In Table 5, we provide the hyperparameters configuration used in our experiments.  
1018

1019 For general changes (aesthetics and complexity), we use positive and negative prompts, following  
1020 the quality-improving prompt modifiers commonly adopted in DMs (Oppenlaender, 2024). In both  
1021 cases, we employ strategy 1 for dynamic modulation guidance with  $w = 3$ , but vary the starting layer.  
1022 Specifically, for complexity, we apply guidance at deeper layers to better preserve the original content  
1023 while refining high-frequency details.

1024 For specific changes (hands correction and object counting), we adopt strategies 1 and 4, as suggested  
1025 by the ablation study. For hands correction, we use simple positive and negative prompts: Natural  
and realistic hands and Unnatural hands. For object counting, the positive direction

1026  
1027  
1028 Table 8: Comparison with baselines for **general changes**. We use Normalized Attention Guidance  
1029 and LLM-enhanced prompts as baselines, and conduct human evaluation on two criteria—**aesthetics**  
1030 and **complexity**—reporting the corresponding win rates.

Model	Variant	Aesthetics		Complexity	
		Baseline	Variant	Baseline	Variant
<i>Baseline: LLM-enhanced prompts</i>					
<b>FLUX schnell</b>	Ours	45	<b>55 (+10)</b>	38	<b>62 (+24)</b>
<b>FLUX schnell</b>	Ours + LLM-enhanced	39	<b>61 (+22)</b>	26	<b>74 (+48)</b>
<b>COSMOS</b>	Ours + LLM-enhanced	41	<b>59 (+18)</b>	35	<b>65 (+30)</b>
<i>Baseline: Normalized Attention Guidance</i>					
<b>FLUX schnell</b>	Ours	33	<b>67 (+34)</b>	21	<b>79 (+58)</b>

1039  
1040 Table 9: Comparison with baselines for **specific changes**. We use Concept Sliders and LLM-enhanced  
1041 prompts as baselines, and conduct human evaluation on two criteria: **defects** for hands correction and  
1042 **text relevance** for object counting, reporting the corresponding win rates.

Model	Variant	Defects, Hands		Text relevance, Counting	
		Baseline	Variant	Baseline	Variant
<i>Baseline: LLM-enhanced prompts</i>					
<b>FLUX schnell</b>	Ours	26	<b>74 (+48)</b>	39	<b>61 (+22)</b>
<i>Baseline: Concept Sliders</i>					
<b>FLUX schnell</b>	Ours	42	<b>58 (+16)</b>	—	—

1053 is adapted per prompt but follows a general structure:  $[n][\text{objects}]$ , where the main object and desired  
1054 count are taken from the prompt.

1055 For text-to-video generation, we use the same configuration as in aesthetics guidance for text-to-image  
1056 generation. We find that this not only makes the videos more realistic but also significantly improves  
1057 their dynamic degree.

1058 For image editing, we adopt the configuration commonly used in CFG: the original prompt serves as  
1059 the positive direction and a blank prompt as the negative. This setup increases editing strength in  
1060 cases where the base FLUX Kontext model struggles. For this setting, we use strategy 1.

## E BASELINES COMPARISONS FOR TEXT-TO-IMAGE GENERATION

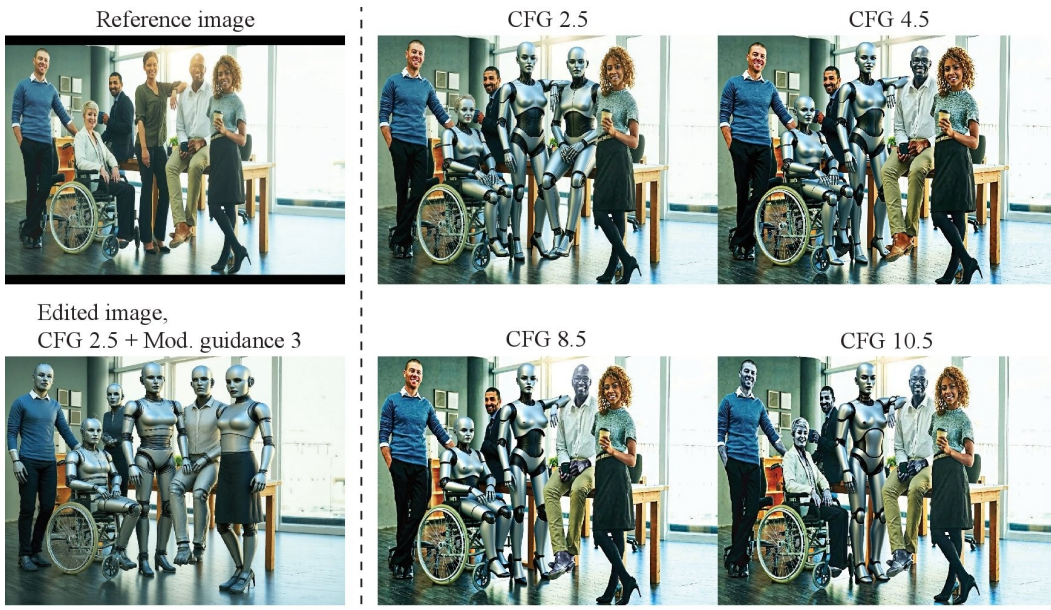
1066 We compare our approach against the following baselines: Normalized Attention Guidance (Chen  
1067 et al., 2025), used for general changes; Concept Sliders (Gandikota et al., 2024), applied to hands  
1068 correction; and LLM-enhanced prompts (Oppenlaender, 2024), which we consider for both general  
1069 and specific changes.

1070 For the LLM-enhanced baseline, we use an LLM to modify the prompt sets by adding additional  
1071 beautifiers, following the same structure used to construct the positive directions in modulation  
1072 guidance. For the other approaches, we adopt the default configurations provided in their respective  
1073 papers.

1074 We present the results for **general changes** in Table 8. We observe significant improvements over  
1075 Normalized Attention Guidance for both criteria (aesthetics and complexity). Importantly, our method  
1076 does not incur additional overhead, unlike Normalized Attention Guidance, which requires extra  
1077 passes through computationally intensive attention layers. Second, we find that our approach can be  
1078 applied on top of LLM-enhanced prompts and brings additional improvements. This is especially  
1079 important in practice, where different modifiers are commonly applied to basic prompts (Ramesh  
et al., 2022).

1080  
1081 Table 10: Comparison of editing performance measured by VLM scores for **Editing Strength** and **Reference**  
1082 **Preservation.**

Configuration	Editing Strength ↑				Reference Preservation ↑			
	Material	Object	Style	Replace object	Material	Object	Style	Replace object
Flux Kontext	66 ±4	78 ±2	68 ±5	71 ±5	93 ±0.1	92 ±0.3	77 ±1	90 ±2
Flux Kontext w/o CLIP	69 (+3)	78 (0)	68 (0)	71 (0)	93 (0)	93 (+1)	79 (+2)	90 (0)
Flux Kontext using final prompt for CLIP	69 (+3)	75 (-3)	68 (0)	73 (+2)	93 (0)	93 (+1)	80 (+3)	89 (-1)
<b>Flux Kontext, modulation guidance</b>	<b>79 (+13)</b>	<b>81 (+3)</b>	<b>72 (+4)</b>	<b>78 (+7)</b>	93 (0)	92 (0)	78 (+1)	89 (-1)

1109 Figure 16: We find that the FLUX Kontext model sometimes struggles with complex image edits, and  
1110 even higher CFG values do not alleviate this issue. In contrast, modulation guidance can effectively  
1111 address such cases.1112  
1113 We present the results for **specific changes** in Table 9. First, we find that our approach outperforms  
1114 the LLM-enhanced prompt baseline on both tasks (hands correction and object counting). Notably,  
1115 for hands correction, the LLM-enhanced prompt approach can lead to divergence—where the model  
1116 overemphasizes hands and neglects other parts of the image. In contrast, our approach localizes model  
1117 attention without adversely affecting the rest of the image. Second, we find that our approach even  
1118 brings improvements over the Concept Sliders approach, without requiring test-time optimization.  
11191120 

## F INSTRUCTION-GUIDED IMAGE EDITING

1121 Here, we present the numerical results for instruction-guided image editing using the FLUX Kontext  
1122 model (Labs et al., 2025). Specifically, we evaluate four settings: (1) the original model; (2) the  
1123 model without CLIP; (3) the model using the final textual prompt instead of the editing instruction  
1124 for CLIP; and (4) the model with modulation guidance. For the latter, we use the final prompt as the  
1125 positive prompt and a blank prompt as the negative, as summarized in Table 5.  
11261127 To evaluate performance, we follow the basic setting of FLUX Kontext and generate images using the  
1128 SEED-Data benchmark (Ge et al., 2024), which provides reference images, editing instructions, and  
1129 final textual prompts. Evaluation is conducted with a VLM model (Bai et al., 2025), which is asked  
1130 to assess editing strength and reference preservation on a 0 – 100 scale. For this purpose, we provide  
1131 the VLM with triples consisting of the reference image, the edited image, and the corresponding  
1132 instruction.  
1133We report the results in Table 10. First, we observe that removing CLIP does not degrade performance  
and even yields small improvements, further supporting our intuition that CLIP does not contribute

1134  
 1135 **Table 11: Performance of text-to-image DMs with and without modulation guidance (gray) on**  
 1136 **Aesthetics and Complexity, evaluated with human preferences and automatic metrics for long and**  
 1137 **short prompts. Human win rates are reported with respect to the original model; green indicates**  
 1138 **statistically significant improvement, red a decline. For automatic metrics, bold denotes improvement**  
 1139 **over the original model.**

Model	Side-by-Side Win Rate, %				Automatic Metrics, COCO 5k			
	Relevance ↑	Aesthetics ↑	Complexity ↑	Defects ↑	PickScore ↑	CLIP ↑	IR ↑	HPSv3 ↑
<b>FLUX schnell, short prompts</b>					21.6	30.1	6.2	7.8
Ours, Aesthetics guidance	49	<b>64</b>	<b>81</b>	<b>57</b>	<b>21.9</b>	<b>30.2</b>	<b>7.4</b>	<b>8.5</b>
<b>FLUX schnell, long prompts</b>					21.0	33.1	10.3	10.8
Ours, Aesthetics guidance	48	<b>60</b>	<b>73</b>	50	<b>21.2</b>	<b>33.3</b>	<b>11.0</b>	<b>11.3</b>

1144  
 1145 meaningful gains. Second, we find that using the final prompt instead of the editing instruction for  
 1146 the CLIP model leads to inconsistent outcomes—improving material and replacement criteria while  
 1147 degrading performance on object editing. Finally, we observe that modulation guidance consistently  
 1148 provides improvements across all criteria in terms of editing strength.

1149  
 1150 Specifically, modulation guidance improves performance on complex editing cases, such as those  
 1151 involving multiple objects. As shown in Figure 16, this problem cannot be solved by simply increasing  
 1152 the CFG scale—only modulation guidance provides improvements.

## 1153 G ADDITIONAL EXPERIMENTS

1154  
 1155 Additionally, we report experimental results for long and short prompts separately to demonstrate  
 1156 that our approach works well with long prompts, whereas basic CLIP tends to influence only short  
 1157 prompts. We conduct a quantitative evaluation using prompts from the MJHQ dataset separated  
 1158 into long and short prompts. We calculate automatic metrics using 1,000 prompts and conducted  
 1159 a human evaluation using 300 prompts. The results are presented in Table 11. We find that our  
 1160 modulation guidance also has a positive impact on long prompts. For instance, human evaluation  
 1161 shows improvements of +20% in aesthetics and +46% in image complexity compared to the original  
 1162 model (FLUX schnell).

## 1163 H LIMITATIONS

1164  
 1165 Our approach also has several limitations. First, it does not address text-to-image correspondence,  
 1166 meaning that it cannot improve how accurately the generated image reflects the input prompt. This  
 1167 limitation is inherent to the modulation guidance design, which focuses on enhancing aesthetic quality,  
 1168 complexity, and other visual attributes rather than semantic alignment. Second, our method introduces  
 1169 a small number of additional hyperparameters that must be tuned to achieve optimal performance.  
 1170 While this tuning process is relatively straightforward, it may add an extra step compared to baseline  
 1171 methods that do not require such configuration.

## 1172 I MORE VISUAL RESULTS

1173  
 1174 We provide additional visual comparisons in Figures 17, 18, 19, 20, 21, 22, and 23.

## 1175 J HUMAN EVALUATION

1176  
 1177 The evaluation is conducted using Side-by-Side (SbS) comparisons, where assessors are presented  
 1178 with two images alongside a textual prompt and asked to choose the preferred one. For each pair,  
 1179 three independent responses are collected, and the final decision is determined through majority  
 1180 voting.

1181  
 1182 The human evaluation is carried out by professional assessors who are formally hired, compensated  
 1183 with competitive salaries, and fully informed about potential risks. Each assessor undergoes de-  
 1184 tailed training and testing, including fine-grained instructions for every evaluation aspect, before  
 1185 participating in the main tasks.

1188  
1189 In our human preference study, we compare the models across four key criteria: relevance to the  
1190 textual prompt, presence of defects, image aesthetics, and image complexity. Figures 24, 27, 25,  
1191 26 illustrate the interface used for each criterion. Note that the images displayed in the figures are  
1192 randomly selected for demonstration purposes.  
1193

## K ADDITIONAL DISCUSSION

1195 This work involves human evaluations conducted through side-by-side image comparisons to assess  
1196 model performance across various criteria (e.g., aesthetics, complexity, and defects). All human  
1197 studies were performed with informed consent, and participants were compensated fairly for their  
1198 time. No personally identifiable information was collected, and all data were anonymized prior to  
1199 analysis. Our research uses publicly available datasets and pre-trained models, adhering to their  
1200 respective licenses and terms of use. While our method aims to improve the quality and controllability  
1201 of generative models, we recognize the potential for misuse of generative technologies, including  
1202 the creation of misleading or harmful content. We encourage responsible use and recommend  
1203 implementing safeguards in real-world applications.

1204 We note that in this paper a large language model (LLM) was used exclusively for polishing the  
1205 writing. It was not employed to generate ideas, methods, or contributions.  
1206  
1207  
1208  
1209  
1210  
1211  
1212  
1213  
1214  
1215  
1216  
1217  
1218  
1219  
1220  
1221  
1222  
1223  
1224  
1225  
1226  
1227  
1228  
1229  
1230  
1231  
1232  
1233  
1234  
1235  
1236  
1237  
1238  
1239  
1240  
1241

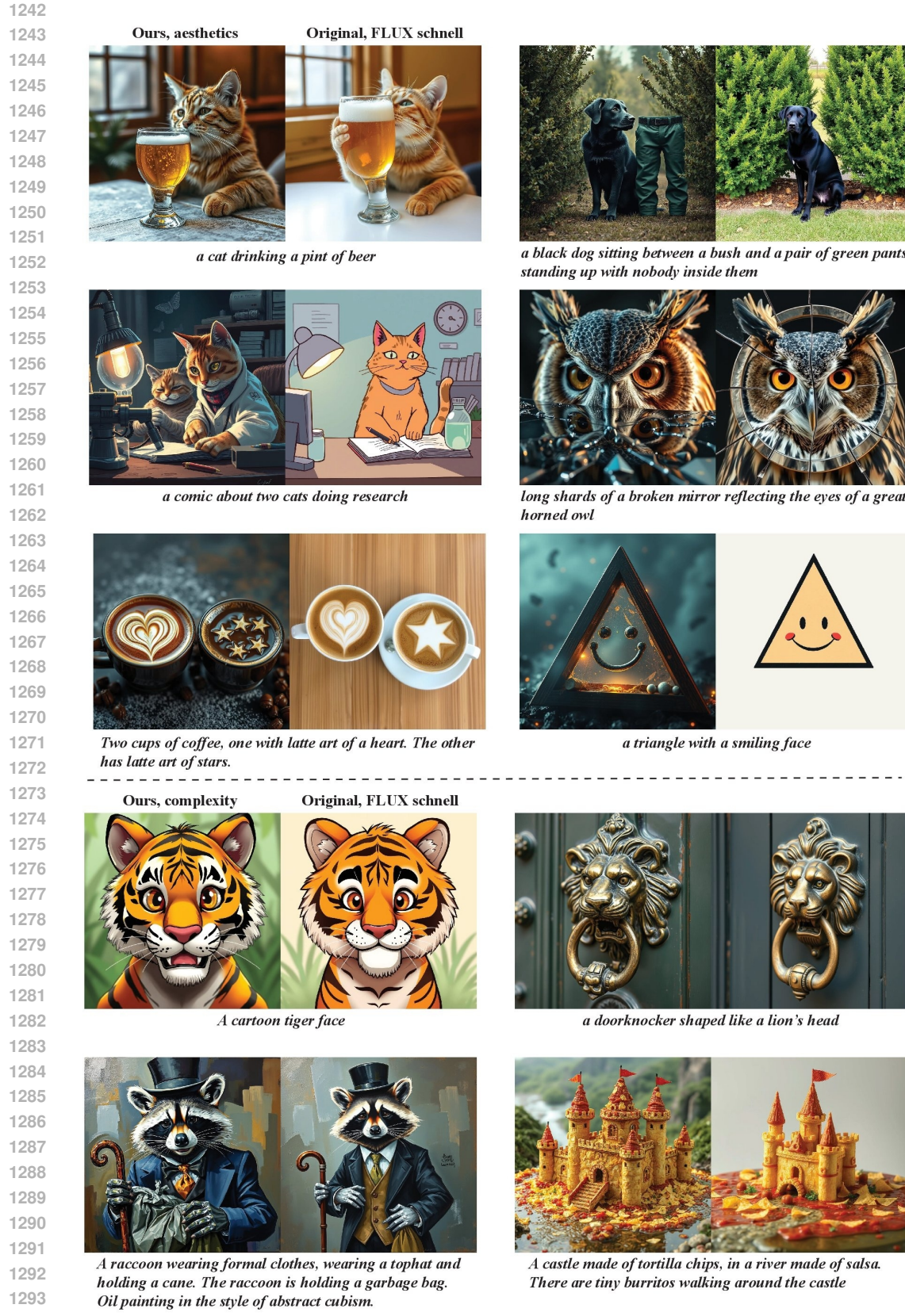


Figure 17: Visual comparisons for FLUX schnell model



Figure 18: Visual comparisons for COSMOS model

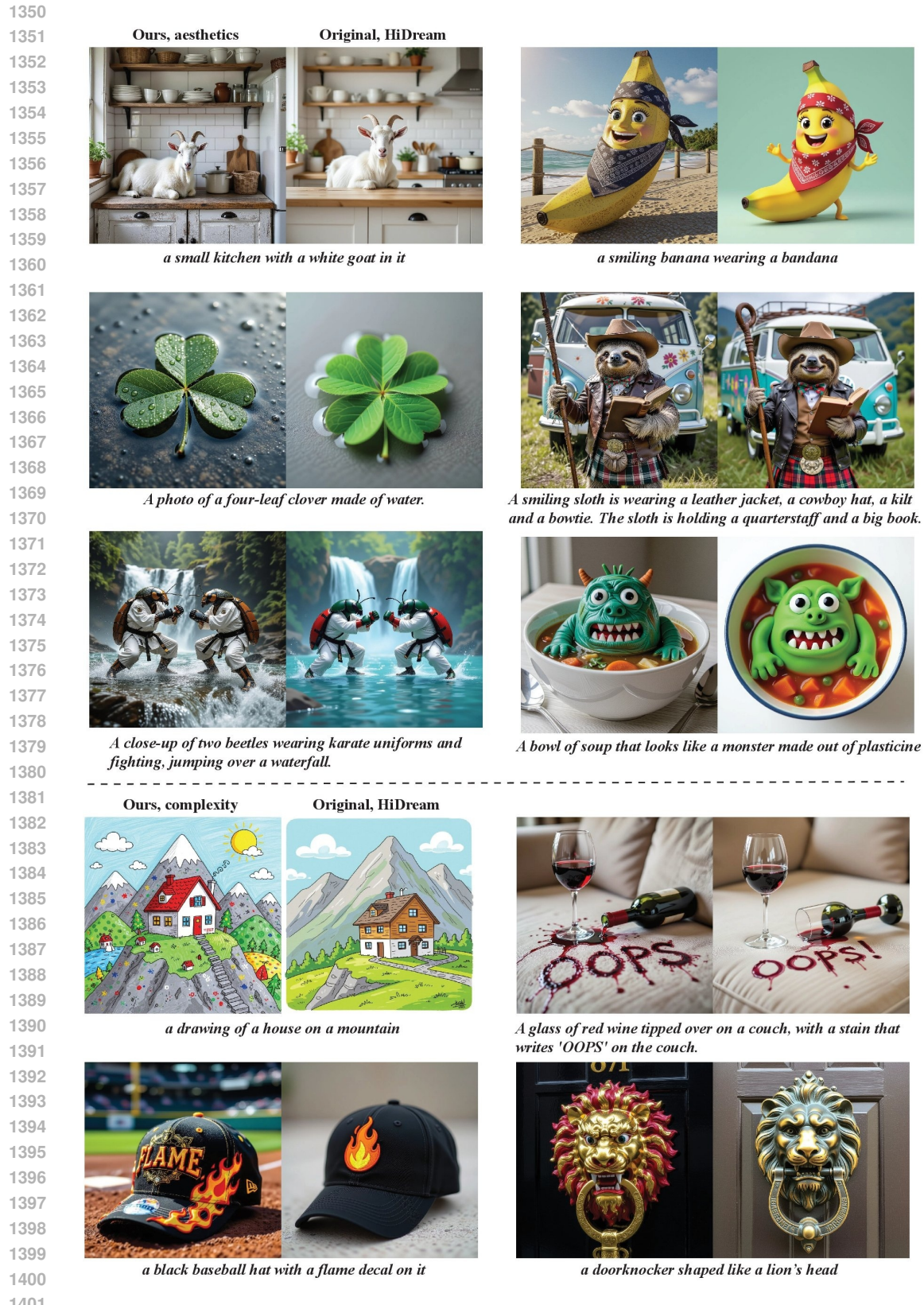


Figure 19: Visual comparisons for HiDream-Fast model

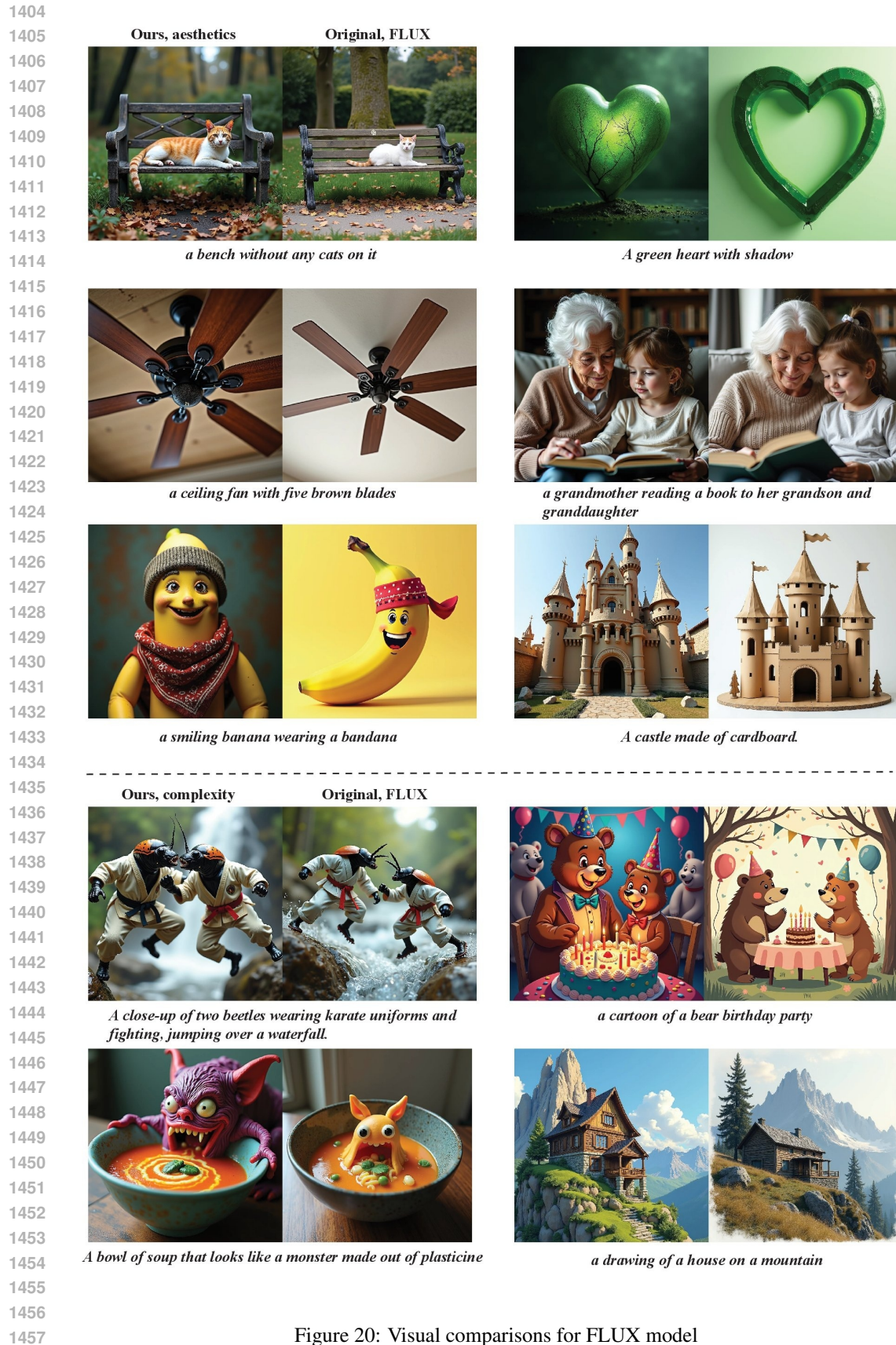


Figure 20: Visual comparisons for FLUX model

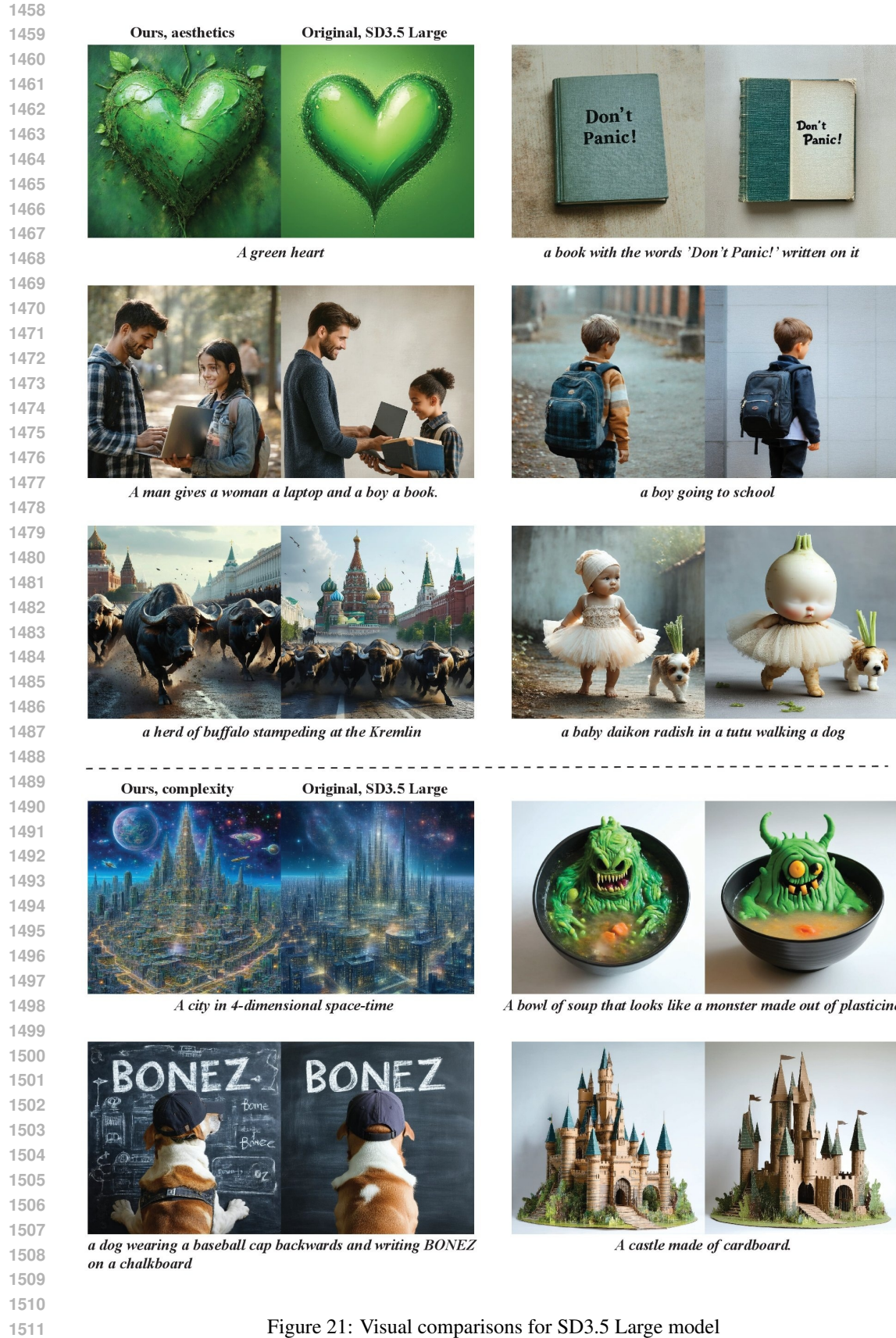


Figure 21: Visual comparisons for SD3.5 Large model

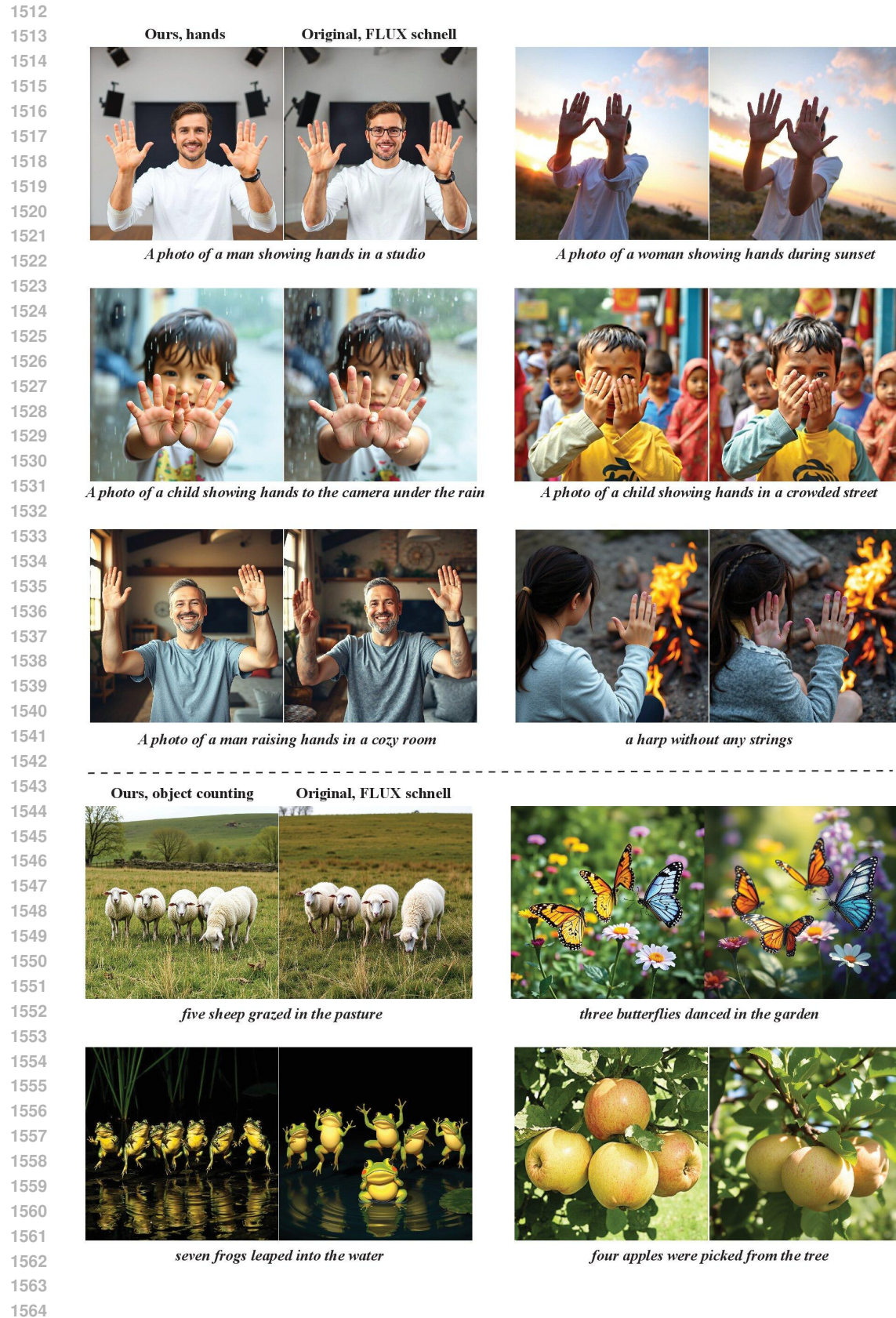


Figure 22: Visual comparisons for FLUX schnell model

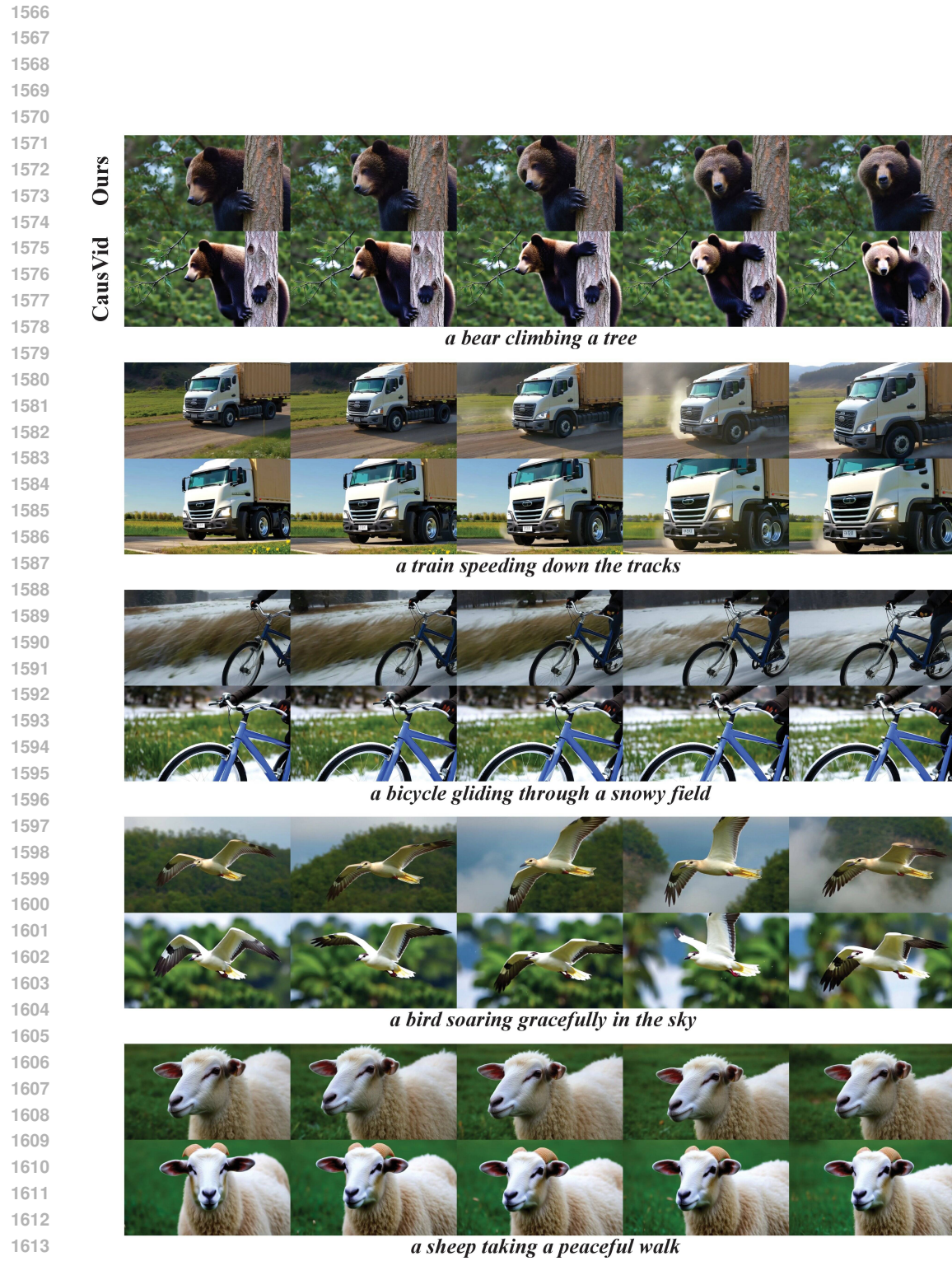


Figure 23: Visual comparisons for CausVid video model

1620  
 1621  
 1622  
 1623  
 1624  
 1625  
 1626  
 Prompt:  
 1627 A medieval Scottish castle with grey stone walls and turrets, positioned next to a mirror-like loch under a misty sky, Highland  
 1628 cows grazing in the foreground, rugged mountains rising in the distance.

1629 Image 1  Image 2 

1630  
 1631  
 1632  
 1633  
 1634  
 1635  
 1636  
 1637  
 1638  
 1639  
 1640 Which image is better according to the instructions?  
 1641  
 1642  9 The images are incomparable  
 1643

1644 Quality: Brightness and contrast      Quality: Acidic and unnatural colors      Quality: Glow  
 1645  
 1646  Image 1 is better       Image 1 is better       Image 1 is better  
 1647  Image 2 is better       Image 2 is better       Image 2 is better  
 1648  The images are equal in this aspect       The images are equal in this aspect       The images are equal in this aspect  
 1649  The images were not evaluated for       The images were not evaluated for       The images were not evaluated for  
 1650 this aspect      this aspect      this aspect  
 1651  
 1652  1 Quality: Image 1 is better  
 1653  2 Quality: Image 2 is better

1654  
 1655 Aesthetics: Visibility of the main      Aesthetics: Background and      Aesthetics: Image detail  
 1656 objects      environment  
 1657  
 1658  Image 1 is better       Image 1 is better       Image 1 is better  
 1659  Image 2 is better       Image 2 is better       Image 2 is better  
 1660  The images are equal in this aspect       The images are equal in this aspect       The images are equal in this aspect  
 1661  The images were not evaluated for       The images were not evaluated for       The images were not evaluated for  
 1662 this aspect      this aspect      this aspect  
 1663  3 Aesthetics: Image 1 is better  
 1664  4 Aesthetics: Image 2 is better  
 1665  8 Can't decide

1666  
 1667  
 1668  
 1669  
 1670  
 1671  
 1672  
 1673

Figure 24: Human evaluation interface for aesthetics.

1674

1675

1676

1677

1678

1679

1680

1681

Prompt:  
an oak door and a cowhide leather belt

1682

1683

Image 1



1684

1685

1686

1687

1688

1689

1690

1691

1692

1693

1694

1695

1696

1697

1698

1699

1700

1701

1702

1703

1704

1705

1706

1707

1708

1709

1710

1711

1712

1713

1714

1715

1716

1717

1718

1719

1720

1721

1722

1723

1724

1725

1726

1727

Image 2



1703

Defects in composition and watermarks

Image 1 is better

Image 2 is better

Images are equal ⓘ

1708

Images style

The images have the same style

The images differ in style / The images are incomparable due to the style ⓘ

The verdict was based on the previous steps

1709

Defects of the main objects

Image 1 is better

Image 2 is better

Can't decide

The verdict was based on the previous steps

1710

Defects of the secondary objects

Image 1 is better

Image 2 is better

Can't decide

The verdict was based on the previous steps

1714

Final answer

1  Image 1 is better

2  Image 2 is better

3  Can't decide

4  The images are incomparable

5  Error loading images

Figure 25: Human evaluation interface for defects.

1728  
 1729  
 1730  
 1731  
 1732  
 1733 **Prompt:**  
 an oak door and a cowhide leather belt

1734 **Image 1** 

1735 **Image 2** 

1736

1737

1738

1739

1740

1741

1742

1743

1744

1745 **Main objects**

1746  there are more main objects in Image 1

1747  there are more main objects in Image 2

1748  both images have the same number of main objects ⓘ

1749

1750 **Final answer**

1751  1 Image 1 is better

1752  2 Image 2 is better

1753  3 Can't decide

1754  4 Error loading images

1755 **Main objects**

1756

1757  there are more main objects in Image 1

1758  there are more main objects in Image 2

1759  both images have the same number of main objects ⓘ

1760

1761 **Secondary objects**

1762  there are more secondary objects in Image 1

1763  there are more secondary objects in Image 2

1764  both images have the same number of secondary objects ⓘ

1765

1766 **Extra objects**

1767

1768  1 Image 1 is better in terms of the effect of extra objects

1769  2 Image 2 is better in terms of the effect of extra objects

1770  3 both images have the same effect of extra objects ⓘ

1771

1772 **Final answer**

1773  1 Image 1 is better

1774  2 Image 2 is better

1775  3 Can't decide

1776  4 Error loading images

Figure 26: Human evaluation interface for relevance.

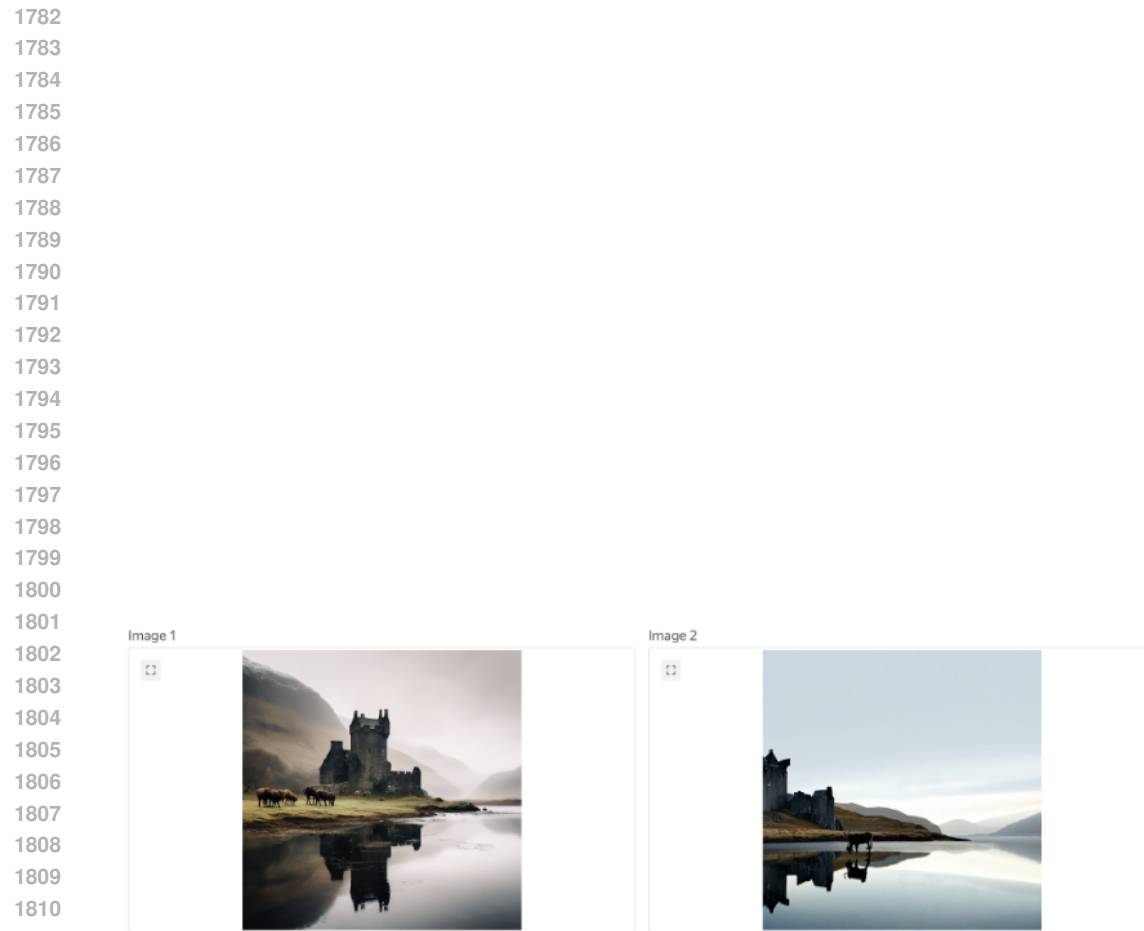


Figure 27: Human evaluation interface for complexity.

1817  
1818  
1819  
1820  
1821  
1822  
1823  
1824  
1825  
1826  
1827  
1828  
1829  
1830  
1831  
1832  
1833  
1834  
1835